Geological Magazine

www.cambridge.org/geo

Original Article

Cite this article: Mitchell RH and Dawson JB (2022) Petrology and Sr–Nd isotope geochemistry of Mosonik: a polygenetic phonolitic nephelinite–phonolite volcano located in the North Tanzanian Divergence of the East African Rift. *Geological Magazine* **159**: 1809–1832. https://doi.org/10.1017/S0016756822000619

Received: 17 December 2021
Revised: 24 May 2022
Accepted: 27 May 2022
First published online: 15 August 2022

Keywords:
Mosonik; phonolitic nephelinite; phonolite; Sr–Nd isotopic relationships; Engaruka melilitites; East African Rift; Tanzania

Author for correspondence: Roger H. Mitchell, Email: rmitchel@lakeheadu.ca

†Deceased 1932–2013

Petrology and Sr–Nd isotope geochemistry of Mosonik: a polygenetic phonolitic nephelinite–phonolite volcano located in the North Tanzanian Divergence of the East African Rift

Roger H. Mitchell[1] and J. Barry Dawson[2,†]

[1]Department of Geology, Lakehead University, Thunder Bay, Ontario, P7B 5E1, Canada and [2]School of Geosciences, Grant Institute, University of Edinburgh, King's Buildings, Edinburgh, Scotland, EH9 3FE, UK

Abstract

Mosonik, a 3.25 Ma extensively dissected stratovolcano located in the North Tanzanian Divergence of the East African Rift, consists predominantly of phonolite and three types of phonolitic nephelinite distinguished by the presence or absence of amphibole or garnet antecrysts and differing populations of complexly zoned antecrystal and phenocrystal pyroxenes. The antecryst–phenocryst assemblage is typical of hybrid lavas derived by magma mixing. Compositional data are given for all major minerals. Owing to the high modal proportions (30–60 vol. %) of antecrysts and phenocrysts of pyroxene and nepheline plus the hybrid character of the lavas, bulk-rock compositions do not represent those of the parental liquids. Thus, assimilation–fractional crystallization modelling of the bulk-rock major- and trace-element abundances is inappropriate and an unevolved parental magma cannot as yet be defined. Sr–Nd isotopic data for Mosonik and other Older Extrusive Series rocks suggest derivation by partial melting of ancient metasomatized lithospheric mantle with mixing of Sr and Nd from two sources coupled with minor lower crustal contamination, melting being induced by the plume currently impinging on the Tanzanian craton, and representing the initial interaction of the plume with the cratonic lithosphere. In contrast, the Younger Extrusives, as exemplified by Oldoinyo Lengai nephelinite–carbonatite volcanism, could be derived from this ancient metasomatized lithospheric mantle plus a recent plume-derived asthenospheric component and no contamination by crustal material. The isotopically and genetically distinct Natron–Engaruka melilitites are considered to represent direct adiabatic melting of the Tanzanian plume without lithospheric contributions. Carbonatites and melilite-bearing nephelinites also occur at Mosonik but are not considered in this study as they are only a very minor volumetric component of the volcano.

1. Introduction

Mosonik is an extinct stratovolcano located (2.61° S; 35.80° E) adjacent to Lake Natron in northern Tanzania at the northern margins of the North Tanzania Divergence (Baker *et al.* 1972) of the East African Rift (Fig. 1). This region is characterized by extensive Neogene-to-Recent volcanism represented by abundant basaltic, nephelinitic, melilititic and carbonatite magmatism ranging in age from *c.* 5.9 Ma (Mana *et al.* 2015) to the current activity in the Oldoinyo Lengai area (Dawson, 2008; Reiss *et al.* 2021).

Mosonik belongs to a group of volcanoes known collectively as the Older Extrusive Series (5.9 Ma to *c.* 3.2 Ma), which are characterized mainly by voluminous alkali olivine basaltic magmatism as exemplified by the major shield volcanoes of Kilimanjaro, Ngorongoro, Gelai and Kitumbeine, with lesser nephelinite–phonolite stratovolcanicity at Sadiman, Shombole, Mosonik and Lemagrut, and peralkaline trachytes at Tarosero. Subsequent to Late Pleistocene time, the eruption style changed to relatively small volume stratovolcanicity at Oldoinyo Lengai, Kerimasi, Meru, Burko, Hanang, Kwahra and the Engaruka–Natron volcanic field, referred to as the Younger Extrusive (<1.2 Ma) Series, with dominant nephelinite, phonolite, melilititic and carbonatite volcanism (Dawson, 2008).

Phlogopite and bulk-rock nephelinite from Mosonik have yielded conventional K–Ar ages of 3.18 ± 0.08 Ma (Isaac & Curtis, 1974), 3.53 ± 0.6 Ma (P. C. Manega, unpub. Ph.D. thesis, Univ. Colorado, 1993) and 4.06 Ma (Muirhead *et al.* 2016), respectively. In this work a new age determination of phlogopite by laser incremental heating ^{40}Ar–^{39}Ar methods using the MAP215-50 instrumental system at the Oregon State University Argon Geochronology Laboratory gave an age of 3.25 ± 0.10 Ma, indicating that Mosonik is one of the youngest volcanic centres of the

Fig. 1. (Colour online) Locations of the major volcanoes in the North Tanzanian Divergence discussed in this work (after Dawson, 2008) (Google Earth © Landsat/Copernicus).

Older Extrusive Series in the North Tanzania Divergence, with Sadiman (4.6–3.3 Ma: Zaitsev *et al.* 2012, 2015) and Essimingor (5.91–5.76 Ma: Mana *et al.* 2012) being considerably older.

Mosonik is located on the up-thrown side of the Natron Basin boundary escarpment near the southern end of Lake Natron (Fig. 2). The volcanic rocks are faulted at their northern margins by the 1.2 Ma N–S-trending Sanjan Fault. In contrast to the Younger Extrusive Series volcanoes, Mosonik (Fig. 2), Shombole and Essimingor are extensively dissected, and well-defined cones are not present. A central caldera is known at Shombole, although at Mosonik and Essimingor there is no evidence for summit craters.

2. Previous studies

Mosonik was first visited by the German geologists Carl Uhlig and Fritz Jaeger in 1904 during a survey of the East African Rift from Lake Manyara to Lake Natron (Uhlig, 1907; Uhlig & Jaeger, 1942). Initially, the volcano was considered to consist of basement or sedimentary rocks and that the unusual morphology was a result of faulting; Uhlig subsequently recognized the presence of volcanic rock but, given that no crater was evident, considered the occurrence to be a fissure eruption. Samples collected were subsequently examined by the eminent petrographers Brögger (1921, pp. 249, 398) and Rosenbusch (1907, p. 1455) and described as 'ringite' (aegirine 'sövite') and sodalite nephelinite, respectively.

N. J. Guest (unpub. Ph.D. thesis, Univ. Sheffield, 1953), during a survey of the geology of the western scarp of the rift, initially recognized the Older and Younger Series of volcanic rocks, and at Mosonik the presence of mela-nephelinite, nephelinite and phonolite together with biotite-bearing grey ash. Subsequently, Guest *et al.* (1961) showed on the Quarter Degree Sheet No. 39 of the Tanzania Geological Survey that Mosonik consisted mainly of nephelinitic–phonolite tuffs and agglomerates, together with an eastern lobe of lava.

Paslick *et al.* (1995, 1996) undertook Sr–Nd–Pb isotope studies of diverse Older and Younger Series volcanic rocks, and presented whole-rock and isotopic compositions for three nephelinites from Mosonik (Paslick *et al.* 1996), together with a sample incorrectly termed a 'basanite' on the basis of classification using the whole-rock composition in terms of total alkali–silica (TAS) volcanic rock nomenclature (Le Maitre *et al.* 2002). Petrographic data to support this designation were not presented. Paslick *et al.* (1995) included at least one sample from Mosonik in their study, although this was not specifically identified as it was grouped with other diverse Older Extrusive rocks. The different sampling number schemes in these papers preclude identification of this material. The isotopic studies indicated isotopic and 'chemical' dis-equilibria in all of the volcanic rocks analysed (see Section 7 below), and no detailed mineralogical study of Mosonik was undertaken, although Paslick *et al.* (1996) presented very limited paragenetic and compositional data for nepheline, titanite, apatite and titanomagnetite.

Dawson (2008, p. 41) summarized the observations of an expedition by J. B. Dawson, A. N. Mariano and R. H. Mitchell to Mosonik in September 2005 as follows. Carbonate-cemented tuffs and lapilli tuffs blanket the lower northern and western slopes of the mountain and cover the plains to the west. Nepheline- and clinopyroxene-phyric lavas and pyroclastic rocks form the bulk of the volcano. Nephelinite *sensu stricto* is not the dominant rock type as most samples contain groundmass alkali feldspar and are hence transitional to phonolite, which is present in small amounts. Zaitsev *et al.* (2015) and Sedova *et al.* (2018) confirmed that the bulk of volcano is composed of diverse phonolitic nephelinites and phonolites and reported that melilite-bearing nephelinite is also present but did not elaborate further on the location of the occurrence.

https://doi.org/10.1017/S0016756822000619 Published online by Cambridge University Press

Some modal data for these lavas were presented by Sedova *et al.* (2018) together with compositional data for resorbed melilite phenocrysts (akermanite–alumino-akermanite), nepheline and pyroxene (see Section 6 below). Xenoliths of mica pyroxenite, ijolite and country rocks (quartzite and schist) occur in the volcanic rocks and are common in the vicinity of the eastern lobe lava.

The Guest *et al.* (1961) survey map shows a small occurrence of carbonatite within the volcanic rocks in a northerly trending valley on the western side of the mountain. This carbonatite was not found by the Dawson 2005 expedition (Dawson, 2008), and neither by M. S. Garson in an unpublished United Nations geological survey report (pers. comm. to Dawson, 2008). However, in September 2007, Dawson & Mitchell (unpub.) observed rare, but inaccessible, blocks of carbonatite in the walls of the gorge of the Leshuta River which drains eastwards from the volcano. Subsequent visits to Mosonik by Anatoly Zaitsev and others in 2009 and 2015 have apparently also been unable to locate the Guest *et al.* (1961) occurrence, perhaps owing to the presence of the extensive vegetation. However, Zaitsev *et al.* (2015) and Sedova *et al.* (2018) reported the presence of small (<0.5 m) boulders of carbonatite in the longest western valley, although no carbonatites were observed in outcrop. Anatoly Zaitsev (pers. comm.) has also confirmed the presence of carbonatite boulders in the Leshuta River gorge and that a dyke of carbonatite, 2–3 m in width and 10 m in length, occurs *in situ* in the southwestern part of the volcano. These occurrences demonstrate that carbonatites are indeed present at Mosonik but their rarity indicates that they are volumetrically not significant. These discoveries suggest that the aegirine 'sövite' described by Brögger (1921) indeed originated from Mosonik.

A summit crater or caldera is not present and the col (2° 34.713′ S; 35° 49.535′ E) is composed of phonolitic nephelinite. It is impossible to produce a detailed geological map of the volcano as the extensive vegetation (Fig. 2) coupled with a predominance of 'wait-a-bit thorns' precludes detailed or extensive traverses. The Leshuta River gorge exposes debris flows and lahars containing mega-xenoliths of Mosonik volcanic rocks.

This manuscript describes volcanic rocks collected by the 2005 Dawson Expedition and presents the results of petrographic and mineralogical studies together with bulk-rock and isotopic compositional data. Some new Sr–Nd isotopic data for Oldoinyo Lengai and the Recent Natron–Engaruka melilitites in the North Tanzanian Divergence are also included in this paper for comparative purposes. There is no description of the melilite-bearing rocks, carbonatites, pyroclastic rocks and ijolite suite xenoliths occurring at Mosonik in this publication.

3. Analytical methods

Quantitative compositions for minerals were obtained using carbon-coated polished thin-sections at Lakehead University using a Hitachi SU-70 field emission scanning electron microscope (FE-SEM) with an accelerating voltage of 20 kV and beam current of 300 pA. Raw X-ray spectra were analysed with an Oxford AZtec 80 mm/124 eV energy dispersive X-ray spectrometer (EDS) using process times of 60–120 s. Standards used were jadeite (Na, Al), wollastonite (Ca, Si), Mn-hortonolite (Mn, Fe, Mg), orthoclase (K, Al), $SrTiO_3$ (Sr, Ti), $BaSO_4$ (Ba, S), zircon (Zr), apatite (P, Ca) and $ThNbO_{12}$ (Nb). Pyroxene, nepheline and feldspar data were recalculated into structural formulae and end-member components using an in-house APL Mineralogical Program. For nepheline and feldspar all Fe was assumed to be Fe^{3+}. For pyroxenes Fe^{2+} and Fe^{3+} were calculated from total Fe on the basis of six atoms of oxygen with all Na expressed as $NaFe^{3+}Si_2O_6$. Garnet data were recalculated into IMA approved end-member components using the Excel program of Locock (2008).

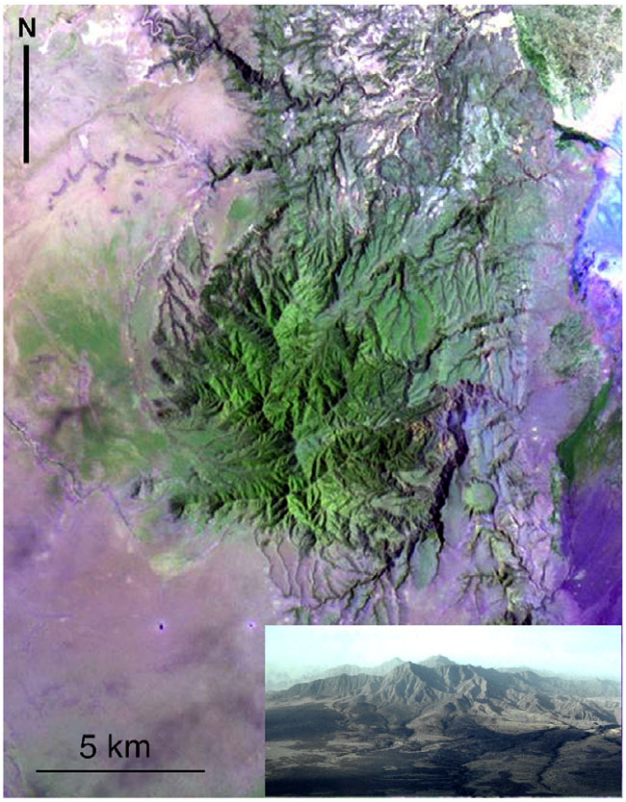

Fig. 2. (Colour online) Google Earth™ satellite image of Mosonik. The inset is an aerial image of Mosonik showing the deeply dissected and extensively forested character of the volcano (Google Earth © Landsat/Copernicus).

Bulk-rock major and trace elements were determined by Activation Laboratories Ltd (Actlabs) at Ancaster (Ontario) using the 4Lithores – lithium metaborate/tetraborate fusion – inductively coupled plasma mass spectrometry package (see online Supplementary Material).

Sr and Nd isotopic compositions for Mosonik were determined at the University of Alberta (see online Supplementary Material) and for Oldoinyo Lengai and Natron–Engaruka at the Memorial University of Newfoundland (see online Supplementary Material). Potassium ^{40}Ar–^{39}Ar ages were determined by laser incremental heating methods at the Geochronology Laboratory of Oregon State University (http://geochronology.ceoas.oregonstate.edu).

4. Petrography of the lavas

Petrographic examination has identified in our sample suite four nepheline-bearing lava types at Mosonik. Three of these contain groundmass alkali feldspar and are best termed phonolitic nephelinites, as they are not nephelinites *sensu stricto*; the fourth lava type is phonolite. The relative proportions of the lava types cannot be determined because of the poor exposure, although Type 2

https://doi.org/10.1017/S0016756822000619 Published online by Cambridge University Press

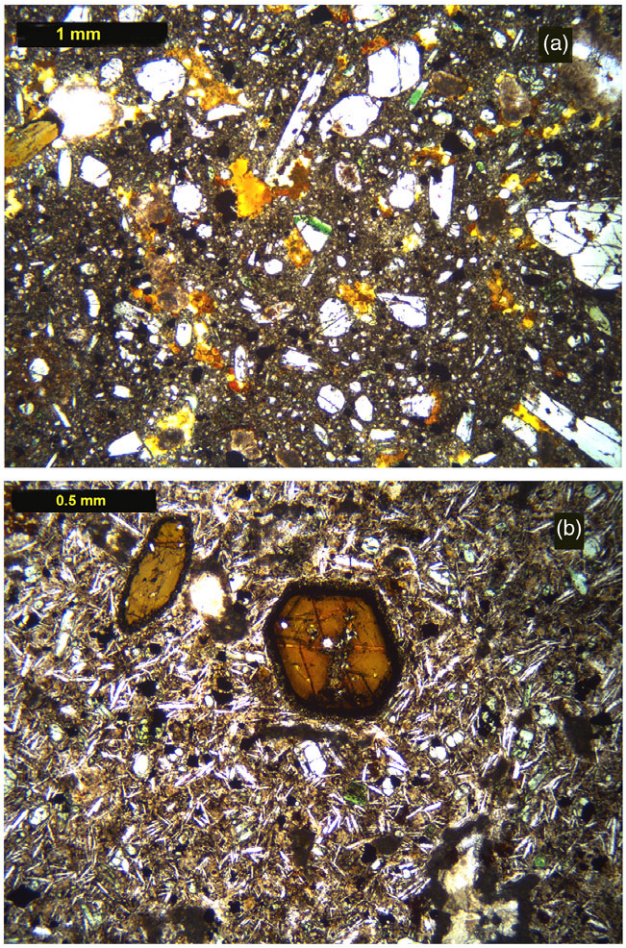

Fig. 3. (Colour online) Photomicrographs of Type 1 lavas: (a) anhedral and euhedral phenocrysts of clinopyroxene some with pale green mantles and anhedral magnetite set in a groundmass of brown altered nepheline, alkali feldspar and orange-red altered glass (MOS28); (b) orange-brown euhedral and subhedral amphibole phenocrysts/antecrysts with opaque reaction rims of very fine-grained diopside and magnetite. The groundmass consists of colourless prismatic alkali feldspar and altered nepheline (MOS23).

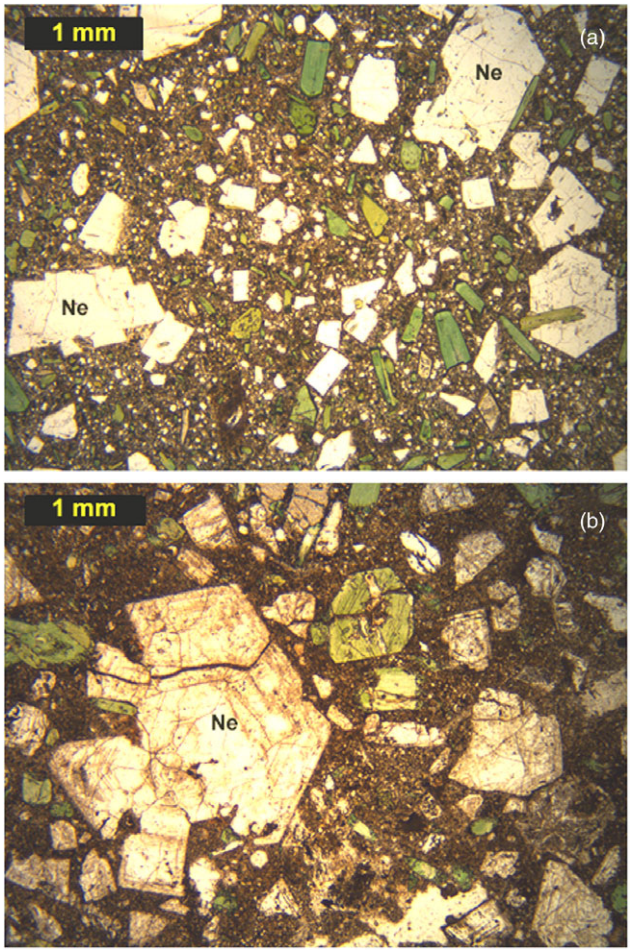

Fig. 4. (Colour online) Photomicrographs of Type 2 lavas: (a) phenocrysts and clasts of nepheline (Ne) together with green prismatic phenocrysts and clasts of clinopyroxene and euhedral titanite set in a brown fine-grained groundmass of clinopyroxene, nepheline and alkali feldspar (MOS13); (b) lava dominated by large complex nepheline phenocrysts (Ne) showing resorption and zoning together with subhedral green zoned clinopyroxene set in a fine-grained optically unresolvable groundmass containing nepheline, sodalite, alkali feldspar and potassium feldspar (MOS24).

nephelinite lavas appear to be dominant. All lavas are antecryst and phenocryst rich (30–60 vol. %), with a heterogeneous population of pyroxenes (see Section 6.a below) indicating that magma mixing has played a significant role in their genesis. Significantly, we thus consider that none of the bulk compositions of the lavas can be considered as representative of liquid compositions. The heterogeneity and alteration of the lavas also precludes the determination of any useful compositional data from the residual fine-grained groundmass.

Type 1 phonolitic nephelinites (Fig. 3) are characterized by anhedral macrocrysts of titanomagnetite, clinopyroxene, clinopyroxene-magnetite intergrowths, round resorbed brown magnesiohastingsite and discrete apatite, together with euhedral phenocrysts of nepheline, K-zeolite pseudomorphs after nepheline and colourless-to-pale brown, euhedral-to-subhedral clinopyroxene. All are set in a groundmass of fine-grained euhedral prismatic alkali feldspar, prismatic clinopyroxene with thin aegirine mantles, zeolitic pseudomorphs after euhedral nepheline, apatite, titanomagnetite, calcite, natrolite, K–Ca-zeolites and altered glass. Amphibole macrocrysts contain rare prismatic crystals of apatite and are not in equilibrium with their current hosts as they have thin-to-near complete reaction mantles of titanomagnetite, diopside-rich clinopyroxene and minor calcite. Vesicles contain calcite and K–Ca-zeolites. Microxenoliths present are phlogopite plus aluminous spinel and ijolite.

Type 2 phonolitic nephelinites (Fig. 4) are characterized by abundant phenocrysts of euhedral-to-subhedral, complexly zoned brown-to-green clinopyroxenes, euhedral nepheline with titanite and clinopyroxene inclusions, and minor titanite. These are set in a fine-grained groundmass of broken and prismatic light green – dark green clinopyroxene with bright green aegirine-rich mantles, acicular Ti-bearing aegirine, euhedral nepheline (20–30 μm) with pseudomorphs of sodalite and/or zeolite, prismatic (10 × 50 μm) alkali feldspar, sodalite, K–Ca-zeolites, calcite and altered glass. Notably absent from Type 2 lavas are groundmass titanomagnetite and the amphibole macrocrysts characteristic of Type 1 lavas, although resorbed macrocrysts (100–300 μm) of apatite are present.

https://doi.org/10.1017/S0016756822000619 Published online by Cambridge University Press

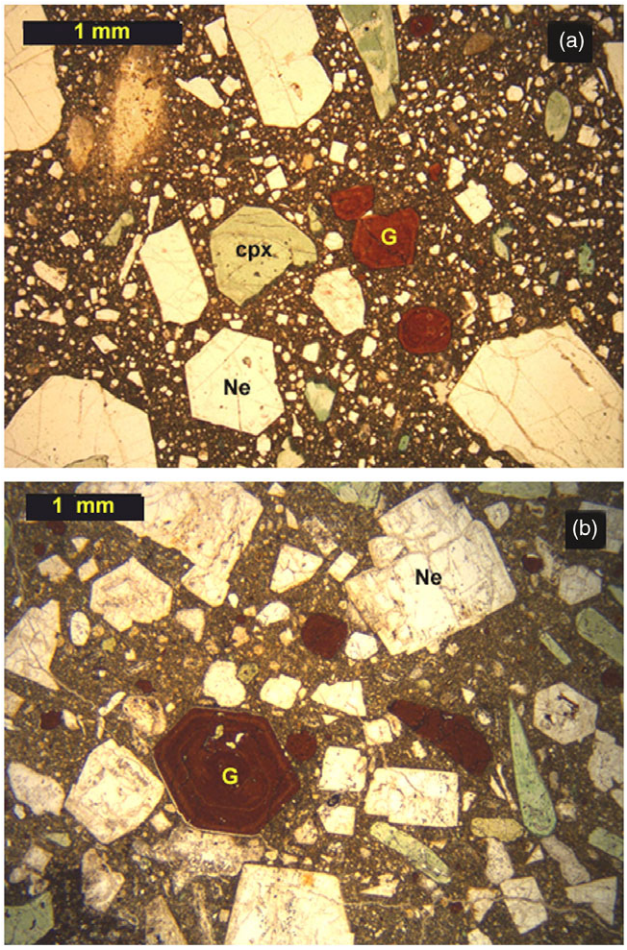

Fig. 5. (Colour online) Photomicrographs of Type 3 lavas: (a) large and small euhedral nepheline (Ne), broken and complexly zoned green clinopyroxene (cpx), rounded red-brown zoned garnet (G) antecrysts set in a very fine-grained brown groundmass of altered and fresh nepheline, alkali feldspar and altered brown glass (MOS 43); (b) crystal-rich lava with euhedral and broken phenocrysts of nepheline (Ne), resorbed phenocrysts of pale green clinopyroxene, euhedral and anhedral red-brown garnet (G) set in a very fine-grained groundmass of green pyroxene altered nepheline, alkali feldspar and altered glass.

Type 3 phonolitic nephelinites (Fig. 5) have many similarities to Type 2 lavas with respect to the overall mineralogy and the occurrence of complexly zoned pyroxenes. They differ principally in that they are characterized by the presence of red-brown subhedral-to-euhedral Ti-rich garnets and nepheline which is enriched in K_2O (see Section 6.c below) relative to that in Type 1 and 2 lavas. Typical Type 3 nephelinite lavas contain garnet, titanite and apatite macrocrysts (up to 500 μm). Phenocrysts include oscillatory zoned nepheline with peralkaline glass inclusions and complexly zoned brown-to-green clinopyroxenes with Ti-aegirine mantles. The groundmass contains euhedral (30–50 μm) nepheline, which is commonly pseudomorphed by sodalite; fresh and altered potassium feldspar; acicular Ti-aegirine; small (<50 μm) prismatic Sr-bearing (1–7 wt % SrO) apatite crystals; K–Ca-zeolites; Na-zeolites and altered interstitial glass. The massive flows at the eastern margin of Mosonik (2° 34.431′ S; 35° 48.860′ E) also contains trace amounts of barytolamprophyllite, fluorite, Sr–Ca–rare earth element (REE) carbonates (bastnaesite and -calcio-ancylite-(La)), fluorite and celestite.

Type 4 lavas are phonolites (Fig. 6) consisting of very large (5–10 mm) euhedral phenocrysts of twin-free or Carlsbad-twinned alkali feldspar and nepheline, with both minerals commonly altered at their margins and along cleavage planes to natrolite, and, in some examples, minor calcite. Alkali feldspars in some instances exhibit marginal incipient microcline twinning. Aggregates of subhedral nepheline are common and some are clearly microxenocrysts of nepheline plus pyroxene. Other phenocrysts include euhedral green complexly zoned or zonation-free clinopyroxene occurring as single crystals which are commonly juxtaposed, indicating magma mixing. Aggregates (0.5–1.5 mm) of subhedral-to-anhedral pyroxene represent fragmented cumulates. Euhedral twinned titanite is a trace phenocryst (<2 vol. %).

The groundmass is extremely fine grained and typically consists of small laths of potassium feldspar, euhedra of nepheline and natrolite pseudomorphs, acicular Ti-bearing aegirine, Sr–REE-bearing apatite, calcite and altered glass. The groundmass is, in some examples, heterogeneous and exhibits a spherulitic texture with ovoid areas of relatively coarse-grained material with pyroxene and titanite microphenocrysts set in a finer grained mineralogically similar groundmass which lacks these minerals. Rare macrocrysts of titano-magnetite are surrounded by Ti-aegirine plus titanite mantles.

5. Bulk-rock geochemistry

The bulk-rock compositions of representative lavas are listed in Table 1 and plotted in the Le Maitre *et al.* (2002) IUGS TAS diagram (Fig. 7). With respect to TAS, many of the Type 1 nephelinite lavas plot in the fields of tephritic lavas regardless of not containing plagioclase. This incorrect nomenclature arises because the rocks do not represent liquid compositions and their modal mineralogy is dominated by calcic, sodic-calcic and sodic pyroxenes. Thus, all Type 1 lavas plot as phonotephrite or tephrite basanite, whereas some Type 4 phonolites plot as tephriphonolite. Type 2 and 3 nephelinite lavas are all essentially foidites in terms of TAS but are mineralogically phonolitic nephelinites.

None of the lavas can be considered as strongly peralkaline, as the peralkalinity index (molar $(Na_2O + K_2O)/Al_2O_3$) ranges from 0.68 to 1.22. Mosonik Type 2 nephelinite lavas are similar to nephelinites from Sadiman (Zaitsev *et al.* 2012) and some Shombole (Peterson, 1989*a*) lavas in terms of TAS (Fig. 7) and peralkalinity (Sadiman 0.88–1.21; Shombole 0.86–1.37), but do not exhibit the wider compositional variation of the Shombole lavas.

With respect to trace elements the lavas are, in common with the major-element variations, heterogeneous (Table 2). Extended mantle normalized trace-element (aka spider diagrams) diagrams for Mosonik lavas are not presented as we consider that these diagrams are not relevant to magmas derived from metasomatized mantle sources (see Section 8 below), and as the whole-rock compositions certainly do not represent those of liquids. The principal trace-element variation is in respect to that of Type 2 and 3 nephelinite lavas relative to types 1 and 4. Surprisingly, the mineralogically least evolved Type 1 nephelinite lavas are, in terms of trace elements, geochemically similar to the most evolved Type 4 phonolites. This dichotomy is well illustrated by the REE chondrite-

https://doi.org/10.1017/S0016756822000619 Published online by Cambridge University Press

Table 1. Whole-rock compositions of Mosonik volcanic rocks

	SiO_2	Al_2O_3	Fe_2O_3	MnO	MgO	CaO	Na_2O	K_2O	TiO_2	P_2O_5	LOI	Total
Type 1												
Mos8	46.31	14.26	12.96	0.21	4.20	7.90	4.79	3.18	21.90	0.59	2.96	99.25
Mos13	47.00	16.43	8.31	0.21	1.54	8.32	9.57	3.94	1.21	0.72	2.38	99.63
Mos18	48.82	14.85	10.58	0.20	3.60	7.07	5.37	3.27	1.42	0.42	3.91	99.50
Mos21	44.91	18.69	7.47	0.22	0.79	6.01	8.89	3.34	0.89	0.19	7.46	98.85
Mos27	53.97	19.05	5.10	0.18	0.46	2.46	7.55	5.86	0.50	0.10	3.63	98.85
Mos28	47.19	12.23	11.32	0.19	4.93	9.23	4.30	2.85	1.51	0.54	4.77	99.06
Mos29	43.85	14.79	11.09	0.22	3.15	10.47	4.81	1.92	1.76	0.56	7.06	99.68
Type 2												
Mos7	46.50	15.85	8.77	0.27	2.93	7.12	7.77	4.06	1.04	0.92	3.66	98.89
Mos9	47.47	20.43	5.78	0.19	0.67	4.09	9.79	4.51	0.55	0.13	5.19	98.81
Mos15	48.41	17.34	6.60	0.20	0.76	6.77	7.59	4.69	0.76	0.40	6.17	99.70
Mos45	44.68	16.24	9.57	0.26	2.42	6.78	9.11	3.38	1.32	0.37	4.87	98.98
Type 3												
Mos26	45.24	16.17	9.56	0.26	1.90	6.78	8.30	4.23	1.13	0.80	4.81	99.16
Mos43	40.96	14.30	10.43	0.20	2.15	11.56	5.47	156	1.75	0.73	9.47	98.00
Type 4												
Mos35	52.99	19.70	4.64	0.12	0.46	2.80	6.85	4.77	0.50	0.14	6.91	99.88
Mos36	52.39	19.86	4.92	0.09	0.48	2.05	9.26	4.40	0.53	0.13	4.91	99.03
Mos37	53.18	20.25	4.78	0.14	0.36	2.04	9.94	4.38	0.51	0.14	3.72	99.45
Mos38	53.64	19.28	4.75	0.14	0.38	3.36	6.34	5.14	0.48	0.15	5.79	99.45
Mos39	51.74	19.97	4.93	0.15	0.47	3.02	8.58	4.92	0.51	0.14	5.26	99.70

LOI – loss on ignition.

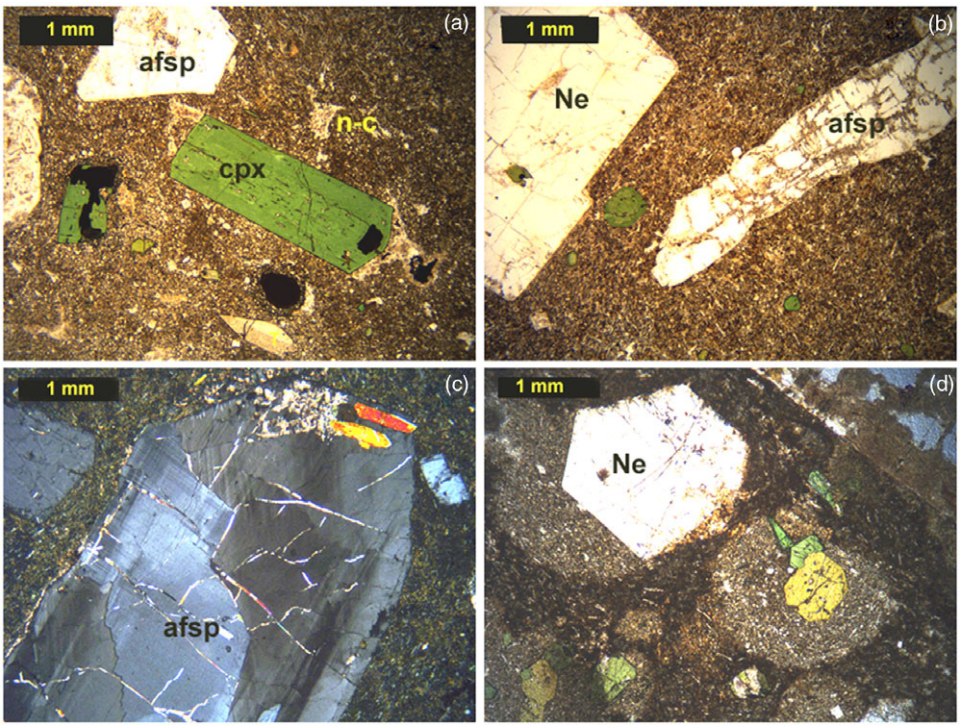

Fig. 6. (Colour online) Photomicrographs of Type 4 lavas: (a) euhedral green clinopyroxene (cpx), colourless alkali felspar (afsp) and twinned titanite (T) phenocrysts set a very fine-grained brown matrix of altered nepheline and alkali feldspar with irregular areas of natrolite and calcite (n-c) (MOS35); (b) large euhedral phenocryst of nepheline (Ne) and resorbed prismatic crystal of alkali feldspar (afsp) with small green phenocrysts of clinopyroxene set in a very fine-grained groundmass of altered and fresh nepheline and alkali feldspar (MOS36); (c) crossed-polarized light image of a typical large phenocryst of alkali feldspar (afsp) showing internal crystallographic domains and incipient microcline twinning (MOS37); (d) heterogeneous groundmass of MOS38 showing the contrast between the globular areas of phenocryst-bearing areas and other regions of the groundmass (MOS39).

https://doi.org/10.1017/S0016756822000619 Published online by Cambridge University Press

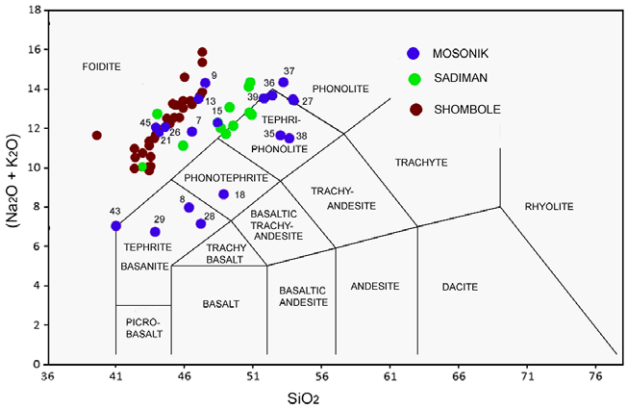

Fig. 7. (Colour online) Total alkali versus SiO_2 (wt %) diagram (TAS) for the major-element bulk compositions of lavas from Mosonik (this work), Shombole (Peterson, 1989*a*) and Sadiman (Zaitsev *et al.* 2012). Mosonik compositions 35–39 are modally phonolites; all other samples are phonolitic nephelinites.

normalized distribution patterns (Fig. 8), which shows that Type 1 and 4 lavas are relatively depleted in overall REE abundances, although having similar distribution patterns to Type 2 and 3 nephelinites. The heavy REE (Tm–Lu) enrichment of the phonolites undoubtedly results from minor crustal contamination as suggested by Sr–Nd isotopic data (see Section 7 below). Europium anomalies are not present and attest to the absence of plagioclase fractionation.

With respect to high field strength incompatible elements (Table 2), there are no significant correlations with lava type excepting that phonolites have overall lower abundances (ppm) of V (29–42), Sr (449–1566), Y (20.5–23.8), Zr (193–230), Nb (72–100), Ba (943–1158) and higher Zr/Nb ratios (2.1–2.9, av. 2.5) than other lavas (875–3638 Sr; 17–44 Y; 148–316 Zr; 64–201 Nb; 1.5–2.8, av. 1.9 Zr/Nb; 701–1735 Ba). The wide variations in the Sr, REEs, Zr and Nb contents (Fig. 9) reflect the extensive variations in antecryst, phenocryst and groundmass clinopyroxene abundance and composition, Y and Zr in garnet, Sr and Ba in alkali feldspar and Sr in calcite as groundmass phases, coupled with 'dilution' by the wide modal variations in nepheline phenocryst content. Because of this complexity none of the trace-element variations can be directly correlated with mineral modal abundances. All lavas are strongly depleted (ppm) in Cu (10–170), Ni (<20), Co (1–41) and Cr (<20).

Compared to Mosonik, the Sadiman lavas (Zaitsev *et al.* 2012) are significantly enriched (ppm) in Sr (1530–2460), Ba (1475–2770), Nb (144–230) and Zr (341–483). Figure 9 illustrates the Nb and Zr enrichment of Sadiman relative to Mosonik. Similar trace-element enrichments (not illustrated) relative to Mosonik occur at Shombole (Peterson, 1989*a*).

6. Mineralogy of the lavas

6.a. Pyroxene compositional variation

Pyroxenes exhibit the greatest compositional variation of all of the minerals occurring in the Mosonik lavas as a consequence of magma mixing and extensive zoning. Overall the compositional range is from diopside through aegirine-augite/aegirine to Ti-bearing aegirine. Representative compositions of pyroxenes in lava types 1–4 are given in Tables 3–6, and the compositional variation in each type illustrated in terms of the diopside–hedenbergite–aegirine (Di–Hd–Ae) ternary solid solution (mol. %) series in Figure 10. Note that these compositional variation diagrams do not illustrate zoning within individual crystals as the intent is to illustrate the overall compositional range of pyroxenes within a particular lava type. Zoning within individual crystals is complex and varies significantly between adjacent crystals. There is no common pattern of either continuous and/or discrete oscillatory zoning and resorption as illustrated in Figure 11, although these define the overall trends shown in Figure 10.

Pyroxenes in Type 1 nephelinite lavas are the least evolved and range principally in composition from $Di_{85}Hd_{10}Ae_5$ to $Di_{60}Hd_{30}Ae_{10}$ (Fig. 10a). One Type 1 lava exhibits a secondary trend originating from the former trend at $Di_{60}Hd_{30}Ae_{10}$ with evolution to $Di_{40}Hd_5Ae_{55}$ (Fig. 10a). These data indicate mixing has certainly played a role in the evolution of the Type 1 nephelinite clinopyroxene phenocryst assemblage. Sedova *et al.* (2018) has reported similar unevolved pyroxene compositions of $Di_{85–53}Hd_{35–10}Ae_{12–4}$ in the melilite nephelinites.

Pyroxenes in Type 2 nephelinites show the greatest compositional variation (Fig. 10b). The least evolved pyroxenes follow the main trend of the Type 1 nephelinite pyroxenes but continue this trend to compositions representing increasing Ae contents at essentially constant low Di contents, i.e. $Di_{85}Hd_{10}Ae_5 \rightarrow Di_{60}Hd_{30}Ae_{10} \rightarrow Di_{10}Hd_{50}Ae_{40} \rightarrow Di_5Hd_5Ae_{90} \rightarrow Ae_{100}$ (Fig. 10b).

Pyroxenes in garnet-bearing Type 3 nephelinites (Fig. 10c) in some respects resemble those in Type 1 and 2 nephelinites. For example, sample MOS43 (Fig. 10c) contains only relatively unevolved pyroxenes similar to those of both Type 1 and Type 2 lava types. In contrast, samples MOS11 and 26 contain Na-rich pyroxenes (Fig. 10c) similar to, but not identical with, evolved Type 2 pyroxenes but with greater Di contents ($Di_{30}Hd_{20}Ae_{50}$ to $Di_{10}Hd_{10}Ae_{80}$). The pyroxene compositions suggest that some, but not all, Type 2 lavas incorporated garnets prior to eruption to form Type 3 lavas, and therefore that there are many discrete batches of Type 2 nephelinite, some of which are more evolved in terms of their clinopyroxene and nepheline (see Section 6.c below) assemblages than others. Note that magnetite- and amphibole-bearing Type 1 lavas do not contain garnet antecrysts and Type 3 lavas lack these minerals.

Pyroxenes in the phonolite Type 4 lava exhibit a range in composition primarily from $Di_{70}Hd_{20}Ae_{10}$ to $Di_{20}Hd_{40}Ae_{40}$ (Fig. 10d). The majority of these data plot at the Ae-rich end of this compositional range but with no distinct trend evident and represent crystals which are only weakly zoned. The less-evolved Di-rich compositions are representative of the rare complexly zoned antecrysts. The groundmass in some instances contains very small acicular aegirine prisms. Compared to clinopyroxenes in the Sadiman phonolites ($Di_{25}Hd_{40}Ae_{35–}Di_5Hd_{35}Ae_{60}$), those from Mosonik are relatively poor in Na. Figure 10e indicates that in both volcanoes the phonolites represent the most evolved lavas.

The compositional trends of clinopyroxenes from Mosonik and Sadiman are compared with those of a variety of volcanic and plutonic alkaline rocks in Figure 12. The positions of these trends reflects differing redox conditions and/or peralkalinity of the parental magmas (Mitchell & Platt, 1982; Mitchell & Vladykin,

https://doi.org/10.1017/S0016756822000619 Published online by Cambridge University Press

Table 2. Trace-element compositions of Mosonik volcanic rocks

No.	8	13	18	21	27	28	29	7	9	15	45	26	43	35	36	37	38	39
Type	1	1	1	1	1	1	2	2	2	2	2	3	3	4	4	4	4	4
V	301	132	198	91	30	273	226	134	52	60	148	222	257	34	29	42	30	32
Co	41	14	32	9	4	39	28	13	5	7	14	13	19	4	4	4	4	4
Cu	90	40	110	30	bld	170	90	20	10	10	30	30	60	10	10	bld	bld	bld
Zn	120	130	130	160	120	120	130	160	160	120	190	180	140	110	120	110	110	160
Ga	25	27	24	31	28	17	23	31	36	28	28	31	24	28	29	28	28	28
Rb	64	81	66	89	102	65	49	102	110	130	101	83	84	93	106	98	119	119
Sr	1505	1392	1479	1880	875	1347	3638	1108	1299	2251	1161	1713	1900	1566	449	582	1315	706
Y	23	29	17	37	21	20	28	41	30	32	42	44	36	22	22	24	21	23
Zr	148	251	103	240	316	121	180	303	275	236	267	200	245	230	227	214	193	219
Nb	64	138	64	136	112	54	87	201	178	138	157	172	145	80	95	100	72	95
Ba	848	898	1156	1563	952	1149	758	701	723	1156	1020	1641	1735	1124	943	888	1158	1009
La	54.9	84.9	59.8	108	49.8	61.9	87.6	120	75.3	118	133	135	120	47.6	48.3	46.1	45.9	45.9
Ce	99.9	147	106	179	85.5	109	151	217	122	196	218	228	201	82.3	82.7	82.0	81.8	81.0
Pr	10.6	14.8	10.5	16.9	8.30	11.2	15.2	22.4	12.6	18.6	21.0	21.5	19.2	7.98	8.41	8.18	7.98	8.17
Nd	38.4	50.4	36.2	55.1	27.9	39.3	52.1	76.6	42.1	60.0	69.5	71.0	64.5	26.5	27.9	27.1	26.6	27.5
Sm	6.61	8.16	5.98	8.52	4.75	6.44	8.71	12.3	6.81	9.19	11.3	11.5	10.6	4.51	4.76	4.66	4.48	4.78
Eu	2.21	2.65	1.87	2.82	1.59	2.06	2.80	3.95	2.26	2.79	3.67	3.81	3.39	1.52	1.59	1.58	1.48	1.57
Gd	5.43	6.33	4.55	6.77	3.87	5.09	6.76	9.43	5.51	6.61	8.38	9.21	8.03	3.58	3.86	3.82	3.42	3.82
Tb	0.84	1.00	0.68	1.14	0.67	0.78	1.03	1.47	0.91	1.07	1.40	1.50	1.30	0.65	0.67	0.70	0.62	0.67
Dy	4.62	5.54	3.64	6.67	3.95	4.12	5.60	8.02	5.36	6.03	7.90	8.30	7.17	4.01	4.04	4.24	3.73	4.12
Ho	0.85	1.03	0.62	1.29	0.76	0.72	1.01	1.46	1.02	1.12	1.46	1.53	1.28	0.79	0.77	0.84	0.72	0.81
Er	2.30	2.80	1.62	3.64	2.21	1.91	2.75	3.97	3.04	3.17	4.08	4.30	3.46	2.38	2.26	2.49	2.12	2.36
Tm	0.32	0.40	0.22	0.49	0.32	0.26	0.37	0.56	0.45	0.45	0.57	0.60	0.48	0.36	0.35	0.37	0.32	0.36
Yb	1.94	2.41	1.30	2.94	1.98	1.60	2.23	3.40	2.68	2.70	3.37	3.51	2.88	2.27	2.19	2.28	2.09	2.28
Lu	0.27	0.33	0.19	0.39	0.27	0.22	0.31	0.48	0.36	0.37	0.46	0.46	0.40	0.33	0.31	0.32	0.31	0.32
Hf	4.0	5.2	3.2	4.5	5.9	3.3	4.7	6.2	5.4	5.1	5.3	5.8	4.9	5.1	4.7	4.8	4.9	4.9
Ta	4.23	9.16	4.45	6.37	5.97	3.91	6.28	9.25	5.46	6.31	7.94	7.91	8.43	6.18	6.32	6.22	5.83	6.38
Th	5.82	17.4	3.59	25.5	10.7	4.56	11.8	30.3	28.6	21.8	20.5	22.9	12.1	12.4	11.7	13.0	12.5	11.6
U	0.38	3.54	0.35	1.80	0.42	0.41	1.39	5.10	2.05	4.81	1.89	11.3	2.45	0.61	0.70	1.17	0.59	0.82

All samples have Cr < 20 ppm; Ni < 20 ppm. Types 1, 2 and 3 are phonolitic nephelinites; Type 4 are phonolites (see text). For analytical information see online Supplementary Material. bld – below limit of detection.

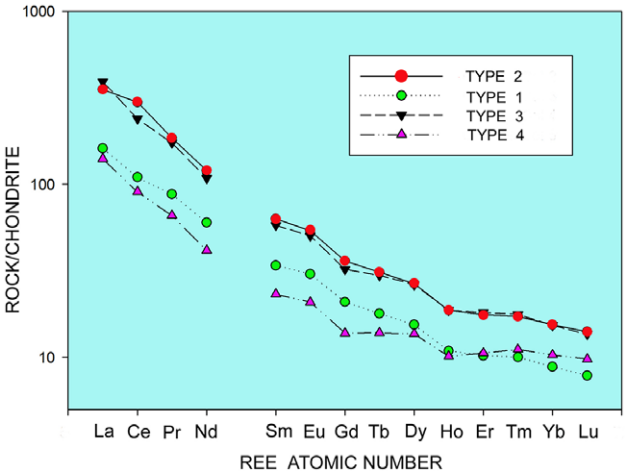

Fig. 8. (Colour online) Chondrite-normalized (Boynton, 1985) rare earth element distribution diagram for representative bulk compositions of Mosonik lava types 1–4.

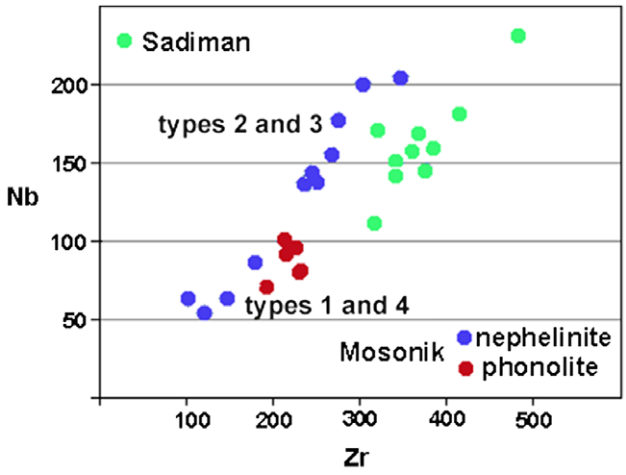

Fig. 9. (Colour online) Nb versus Zr (ppm) relationships for lavas from Mosonik (this work) and Sadiman (Zaitsev *et al.* 2012).

1996). In this context, neither Mosonik nor Sadiman can be considered as being particularly peralkaline or formed under exceptionally high or low oxygen fugacities. The trends of both suites are very similar to those of volcanic rocks from Uganda (Fig. 12: trends 1 and 2).

6.b. Garnet compositional variation

Garnets in Type 3 nephelinite lavas are enriched in TiO_2 and Fe_2O_3 (Table 7) and exhibit a significant compositional range within the morimotoite–andradite–schorlomite (Mmt–Adr–Slo) ternary solid solution series (Fig. 13). The majority of compositions are morimotoite–andradite ranging from $Mmt_{65}Andr_{10}Slo_{25}$ to $Mmt_{30}Andr_{35}Slo_{35}$, reflecting decreasing TiO_2 and increasing Fe_2O_3 contents from core to rim of subhedral crystals. Garnets with oscillatory zoning exhibit the same compositional trend within each zone. Similar Ti-bearing garnets are found at Sadiman (Zaitsev *et al.* 2012) and Shombole (Peterson, 1989*a*). All garnets contain only trace contents of ZrO_2 (<0.3 wt %) in common with other volcanic morimotoite garnets at Sadiman (0.2–0.4 wt % ZrO_2).

6.c. Nepheline, sodalite and feldspar compositional variation

Nepheline in all lava types does not exhibit significant major-element compositional variation, and there are no significant differences between phenocrystal and groundmass nepheline compositions (Fig. 14; Table 8). The principal compositional variation is that of K_2O, with nepheline in individual lavas being distinctive, e.g. Type 1 nephelinite lavas 4.8–5.6 wt %; Type 2 nephelinite lavas MOS15 and MOS10 with 4.2–5.4 wt % or 5.7–6.5 wt %, respectively. Nephelines in Type 3 nephelinite lavas are relatively enriched in K_2O (6.1–7.9 wt %) and those in phonolites relatively depleted (2.8–4.2 wt %). With respect to minor elements, all nephelines lack Ca but contain significant amounts of Fe, with groundmass types being relatively enriched (2–4.5 wt % Fe_2O_3) compared to phenocrysts (0.7–1.8 wt % Fe_2O_3). Where zoning of phenocrysts is evident, crystal margins are enriched in Fe relative to cores. Sedova *et al.* (2018) has noted that nepheline phenocrysts in the melilite nephelinite are relatively potassic ($Ne_{70-66}Ks_{31-8}Qtz_{0-0.1}$).

Groundmass nepheline is commonly partially-to-completely pseudomorphed by sodalite in many of the lavas whose composition (wt %; 25.1 Na_2O; 29.0 Al_2O_3; 38.6 SiO_2; 1.8 Fe_2O_3; 0.3 K_2O; 6.14 Cl; 0.5 S; 99.40 Total) does not vary significantly. Sodalite in turn can be replaced by natrolite (13.78 Na_2O; 22.08 Al_2O_3; 53.8 SiO_2 wt %) and unidentified K–Na–Ca zeolites.

Feldspar occurs principally as a groundmass mineral in most lavas, and only the phonolites are characterized by common phenocrystal feldspar. In contrast to nepheline, feldspars exhibit considerable compositional variation (Fig. 14; Tables 9, 10). Groundmass feldspars in Type 1 lavas show the most extensive composition, and individual lavas are characterized by distinct groundmass feldspar compositions. In one amphibole-bearing lava (MOS23) these are zoned from anorthoclase cores ($Ab_{71}Or_{18}An_{11}$–$Ab_{66}Or_{27}An_7$) to Ca-free albitic feldspar ($Ab_{72}Or_{28}$–$Ab_{56}O_{44}$). Other Type 1 nephelinite lavas contain feldspars ranging in composition from $Ab_{55}Or_{45}$–$Ab_{41}Or_{59}$ in sample MOS31 to $Ab_{22}Or_{78}$–$Ab_{16}Or_{84}$ in MOS25. Feldspars in Type 2 and 3 nephelinite lavas are more 'evolved', in terms of increased K-content, with respect to the Type 1 lava trend of feldspar compositions, and lack anorthoclase and albite-rich types. These range from $Ab_{27}Or_{73}$–Ab_9Or_{91} in Type 2 lavas to Type 3 lavas having a restricted range of potassic feldspar compositions of Ab_5Or_{95}–Ab_3Or_{97} (Fig. 14). One Type 2 lava contains rare (<1 vol. %) phenocrystal alkali feldspar ($Ab_{50-48}Or_{50-52}$) mantled by clinopyroxene. Phenocrystal and groundmass feldspars in the phonolites range from $Ab_{77}Or_{23}$–$Ab_{66}Or_{34}$ and $Ab_{41}Or_{59}$–Ab_5Or_{95}, respectively. Note that the phonolite feldspar phenocrysts are of similar composition in terms of their albite component to those of groundmass anorthoclase in Type 1 lavas but lack CaO.

6.d. Magnetite

Groundmass Ti-magnetite occurs only in Type 1 nephelinite lavas principally as opaque euhedral-to-subhedral 5–50 μm single crystals. Less common larger crystals (50–200 μm) typically exhibit convoluted resorbed margins and embayments. Some magnetite occurs intergrown with groundmass pyroxene in

https://doi.org/10.1017/S0016756822000619 Published online by Cambridge University Press

Table 3. Representative compositions of pyroxene in Mosonik Type 1 nephelinites (MOS29, 18)

wt %	1	2	3	4	5	6	7	8
SiO_2	52.81	51.05	51.93	50.56	51.85	50.70	51.01	49.27
TiO_2	1.02	1.43	0.97	1.49	0.65	1.21	0.49	0.88
Al_2O_3	1.70	2.78	2.27	3.47	1.30	1.90	1.56	1.46
Fe_2O_3	1.91	2.50	2.94	3.09	3.94	4.74	6.03	9.04
FeO	6.28	6.27	6.51	7.32	7.07	8.79	0.83	13.82
MnO	–	–	0.25	0.32	0.11	0.33	0.41	0.74
MgO	13.51	12.46	12.14	11.29	12.59	10.36	6.11	4.51
CaO	23.11	22.43	22.23	22.16	21.72	21.57	18.74	16.69
Na_2O	0.74	0.97	1.14	1.20	1.53	1.84	2.34	3.51
Total	101.08	99.89	100.38	100.90	100.76	101.44	99.52	99.13
Mol. %								
Cats	2.85	4.05	2.76	4.20	1.80	3.37	1.23	2.65
Tsch	0.11	1.48	1.45	3.38	–	–	–	0.53
Ae	5.33	7.08	8.36	8.72	10.91	13.22	18.41	27.28
Wo	44.54	42.50	42.93	40.70	41.90	41.15	40.11	34.25
Fs	9.69	9.89	10.29	11.76	10.88	13.63	21.77	21.82
En	37.47	34.99	34.22	31.54	34.52	28.63	18.48	13.48
Ternary mol. %								
Ae	5.65	7.69	8.87	9.68	1.52	13.84	18.66	28.40
Di	74.96	71.96	70.06	66.24	67.28	58.37	37.44	27.30
Hd	19.39	20.35	21.06	24.08	21.20	27.79	44.00	4.22

Cats = $CaTiAl_2O_6$; Tsch = $CaAl_2SiO_6$; Ae = $NaFe^{3+}Si_2O_6$; Wo = $Ca_2Si_2O_6$; Di = $CaMgSi_2O_6$; En = $Mg_2Si_2O_6$; Hd = $CaFe^{2+}Si_2O_6$. FeO and Fe_2O_3 calculated from total FeO by assigning all Na_2O to $NaFe^{3+}Si_2O_6$.

reaction mantles formed on amphibole antecrysts. Ilmenite exsolution is absent. Magnetite crystallizes prior to groundmass feldspars.

The magnetites are principally Cr-free, Al- and Mg-poor members of the Mn_2TiO_4–Fe_2TiO_4–Fe_3O_4 (MnUsp–Usp–Mt) solid solution series (Table 11). Those occurring in individual Type 1 nephelinite lavas exhibit a range in composition, e.g. $MnUsp_{1-4}UsP_{41-55}Mt_{42-54}$ in sample MOS25. They typically show Ti-enrichment from cores to margins, although there is no correlation between crystal morphology and composition. The principal inter-lava variation is in respect to MgO and MnO: e.g. MgO <0.7 wt % and MnO 0.8–2.2 wt % in sample MOS25; MgO 1.3–3.0 wt % and MnO 0.6–1.0 wt % in sample MOS31; MgO <0.5 wt % and MnO 0.8–1.0 wt % in sample MOS25.

6.e. Amphibole

Amphiboles are present only in Type 1 nephelinite lavas. These occur as isolated round light-green-to-brown antecrysts with complex thin reaction mantles of diopsidic pyroxene and Ti-magnetite with subsequent overgrowths (Fig. 3b) of coarser Ti-magnetite, calcite and pyroxene. The latter are similar in composition ($Di_{71}Hd_{23}Ac_6$–$Di_{65}Hd_{22}Ac_{13}$) to phenocrystal and groundmass pyroxenes in Type 1 lavas (Fig. 10). The amphiboles are all Ti-bearing magnesio-hastingsite and typically continuously zoned with increasing FeO from core to rim (Table 12). Inclusions of apatite are present in some crystals.

6.f. Accessory minerals

Titanite occurs as isolated euhedral phenocrysts (200 μm) in all lavas (<1 vol. %) and as rare euhedral inclusions in nepheline phenocrysts. The composition is near stoichiometric with only minor FeO_T (1–2 wt %) and Nb_2O_5 (<1 wt %) being present. F-bearing (2.3–3.2 wt %) apatite occurs as oval crystals (100–500 μm) in Type 2 and 3 lavas. SrO contents range from 0.7 to 1.9 wt % and REE contents are typically not detectable.

Sr–F-bearing barytolamprophylite ($(Na,K)_2(Ba,Sr,Ca)_2(Ti,Fe)_3(Si_2O_7)_2(O,OH,F)_4$) occurs as a trace (<<1 vol. %) late-stage interstitial groundmass mineral (5–20 μm) and as thin (<5 m) rims on garnet antecrysts in the Type 3 eastern lava flow. Representative compositions are given in Table 13. The groundmass also contains trace amounts of a Sr–REE–F carbonate as irregular patches (<15 μm) in the interstices between feldspars. This mineral cannot be unambiguously identified and requires further characterization. The mineral is unusual as its composition (wt %: 32–33 La_2O_3; 9.5–11.0 SrO; 10.6–11.3 Nd_2O_3; 4.0 Pr_2O_3; 1.9–2.2 F), is dominated by Sr, Nd and La, and contains

https://doi.org/10.1017/S0016756822000619 Published online by Cambridge University Press

Table 4. Representative compositions of pyroxene in Mosonik Type 2 nephelinite lavas

wt %	1	2	3	4	5	6	7	8
SiO_2	49.71	50.73	50.19	49.85	51.13	52.38	50.77	49.99
TiO_2	1.47	1.14	0.85	0.66	0.59	0.63	1.88	4.31
Al_2O_3	3.03	2.22	1.56	0.95	1.76	1.08	1.18	1.11
Fe_2O_3	2.32	2.58	3.50	5.77	6.11	7.06	16.13	24.86
FeO	5.78	7.99	11.57	14.28	12.69	10.58	7.62	1.16
MnO	0.21	n.d.	0.30	0.53	0.62	0.53	0.37	0.36
MgO	12.78	11.69	8.85	5.75	6.17	6.53	3.67	1.65
CaO	23.15	23.11	21.34	19.70	19.39	18.66	13.31	6.93
Na_2O	0.90	1.00	1.36	2.24	2.37	2.95	6.26	9.65
Total	99.35	100.46	99.52	99.73	100.83	100.40	101.19	100.02
Mol. %								
Cats	4.14	3.19	2.47	1.95	1.79	0.62	2.72	2.68
Tsch	0.63	0.24	0.54	–	0.62	–	–	–
Ae	6.53	7.22	10.18	17.10	18.24	22.80	47.53	76.53
Wo	44.62	44.41	42.65	40.57	40.03	39.54	26.56	13.85
Fs	9.05	12.45	18.68	23.50	21.03	17.64	12.47	1.91
En	35.64	32.47	25.48	16.88	18.26	19.40	10.71	5.03
Ternary mol. %								
Ae	6.90	7.52	10.67	17.47	18.83	23.53	50.62	84.54
Di	74.25	66.85	51.55	34.49	37.70	36.41	22.82	11.23
Hd	18.85	25.63	37.78	48.04	43.47	40.06	26.56	4.23

Cats = $CaTiAl_2O_6$; Tsch = $CaAl_2SiO_6$; Ae = $NaFe^{3+}Si_2O_6$; Wo = $Ca_2Si_2O_6$; Di = $CaMgSi_2O_6$; En = $Mg_2Si_2O_6$; Hd = $CaFe^{2+}Si_2O_6$. n.d. – not detected. FeO and Fe_2O_3 calculated from total FeO by assigning all Na_2O to $NaFe^{3+}Si_2O_6$.

minor amounts of other REE_2O_3 but lacks Ce (<0.3 wt % Ce_2O_3), perhaps due to removal as Ce^{4+}. Possible minerals are Ce-deficient ancylite-(La) or Sr-kozoite-(La).

6.g. Peralkaline glass inclusions in nepheline

Phenocrystal nephelines in some Type 3 lavas contain 15–30 μm spherical inclusions consisting principally of silicate glass. Former gas bubbles and wollastonite crystals are present in some examples and carbonates are apparently absent. Table 14 shows that, although the glass is of diverse composition, all examples are strongly peralkaline, with peralkalinity indices ranging from 6.25 to 13.35, iron-enrichment and significant Cl and S contents. Fluorine is also present but cannot be quantitively determined by EDS methods in the presence of significant amounts of Fe. These data and the presence of barytolamprophyllite suggest that the development of peralkaline lavas might be possible at Mosonik.

7. Sr–Nd isotopic relationships

New data for the bulk-rock Sr and Nd isotopic compositions for Mosonik volcanic rocks are given in Table 15 and illustrated in Figures 15–17. Because of the young age of the rocks, their low Rb/Sr and low Sm/Nd ratios coupled with high Sr contents, the isotopic data are not age corrected and are considered to represent initial ratios. Table 15 and Figure 15 indicate that for data obtained in this work there is no correlation between lava type and isotopic compositions. The lavas have distinctly different Sr and Nd isotopic compositions, and Figure 15 shows that all Nd isotopic compositions ($\epsilon_{Nd}(0)$ −3.1 to −8.3) plot below the present day bulk earth chondritic uniform reservoir (CHUR) Nd isotopic composition ($\epsilon_{Nd}(0)$) implying derivation from an old source enriched in the light REEs (low Sm/Nd) relative to bulk earth, suggesting derivation from depleted mantle sources. Sr isotopic compositions straddle the chondritic bulk earth composition ($^{87}Sr/^{86}Sr = 0.7047$) but are not significantly enriched in radiogenic Sr, suggesting sources possibly with low Rb/Sr ratios and no crustal contamination. Mosonik compositions all plot below the field of Oldoinyo Lengai silicate lavas (Bell & Peterson, 1991), which are coincident within the East African Carbonatite Line (Bell & Blenkinsop, 1987).

Figure 15 also shows Sr–Nd isotopic compositions for four lavas from Mosonik determined by Paslick *et al.* (1996). These differ significantly from those determined in this work as they plot above the bulk earth CHUR Nd isotopic composition with $\epsilon_{Nd}(0)$ +0.86 to +1.81 and lower $^{87}Sr/^{86}Sr$ ratios close to the East African Carbonatite Line. These differences are unlikely to

https://doi.org/10.1017/S0016756822000619 Published online by Cambridge University Press

Table 5. Representative compositions of pyroxene in Mosonik Type 3 nephelinite lavas

wt %	1	2	3	4	5	6	7	8
SiO_2	50.03	50.43	50.15	50.97	52.11	50.65	50.13	49.63
TiO_2	0.93	0.89	0.79	0.46	0.62	0.51	4.92	4.42
Al_2O_3	2.52	1.35	1.17	1.18	1.12	2.90	0.73	0.83
Fe_2O_3	3.04	3.74	4.87	7.96	7.57	23.73	13.39	15.80
FeO	8.59	9.13	9.45	11.30	10.14	3.19	9.03	7.80
MnO	0.25	0.31	0.43	0.44	0.33	0.38	0.20	0.23
MgO	10.45	9.84	8.94	5.96	7.52	1.82	4.15	3.78
CaO	22.57	22.08	21.30	18.93	19.00	7.98	12.00	11.91
Na_2O	1.18	1.45	1.89	3.09	2.94	9.21	6.98	7.18
Total	99.56	99.22	98.99	100.29	101.35	100.37	101.53	101.58
Mol. %								
Cats	2.66	2.56	2.29	1.35	1.62	1.50	1.70	1.91
Tsch	1.72	–	–	0.91	–	3.79	–	–
Ae	8.69	10.76	14.10	23.41	21.98	70.04	53.50	54.36
Wo	43.72	43.99	42.77	38.50	38.43	14.12	24.56	23.96
Fs	13.64	14.61	15.20	18.46	16.35	5.23	8.01	8.77
En	29.58	28.08	28.65	17.36	21.61	5.32	12.23	11.00
Ternary mol. %								
Ae	9.13	11.19	14.72	24.63	22.45	76.85	56.92	57.88
Di	62.18	58.42	53.54	36.53	44.17	11.68	26.03	23.43
Hd	28.69	30.39	31.74	38.84	33.38	11.47	17.05	18.69

Cats = $CaTiAl_2O_6$; Tsch = $CaAl_2SiO_6$; Ae = $NaFe^{3+}Si_2O_6$; Wo = $Ca_2Si_2O_6$; Di = $CaMgSi_2O_6$; En = $Mg_2Si_2O_6$; Hd = $CaFe^{2+}Si_2O_6$. FeO and Fe_2O_3 calculated from total FeO by assigning all Na_2O to $NaFe^{3+}Si_2O_6$.

be attributed to analytical errors as data presented for Nd and Sr isotopic standards (Table 15) indicate satisfactory inter-laboratory analytical accuracy and precision between the Universities of Alberta and Michigan analytical protocols. These data significantly extend the extent of Sr–Nd isotopic variation at Mosonik (see below).

Figure 15 also illustrates Sr and Nd isotopic data for nephelinites and phonolites from Shombole (Bell & Peterson, 1991), a petrologically similar Older Extrusive volcano (1.96–2.0 Ma; Fairhead *et al.* 1972; Peterson, 1989*a*) adjacent to Mosonik. These volcanic rocks are similar to those of Mosonik in having a wide range in initial negative $\epsilon_{Nd}(0)$ isotopic compositions. However, they differ with respect to Sr in having much lower initial $^{87}Sr/^{86}Sr$ ratios. These data suggest that Mosonik and Shombole lavas are derived from different sources or from similar sources which have undergone different genetic processes, such as different styles of metasomatism. Unlike Shombole, there is no significant correlation between $^{143}Nd/^{144}Nd$ and the SiO_2 contents of Mosonik lavas. At Mosonik and Shombole $^{87}Sr/^{86}Sr$ ratios are not correlated with SiO_2.

Figure 16 illustrates Sr and Nd isotopic compositions of Older Series Volcanics in the North Tanzania Divergence (Paslick *et al.* 1995, 1996; Mana *et al.* 2015; Zaitsev *et al.* 2019) and shows that each volcanic centre has a distinct isotopic composition. The majority of these data, including the Paslick *et al.* (1996) data for Mosonik, are isotopically different from the new data for the Mosonik volcanics, with only lavas from Sadiman (Zaitsev *et al.* 2019) and some lavas from Essimingor and Lemagrut having relatively similar isotopic compositions to the Mosonik lavas analysed in this work. However, considering the extreme isotopic variation of the Mosonik lavas indicated by inclusion of the Paslick *et al.* (1995, 1996) data, note that the Essimingor and Monduli lavas exhibit a similar wide range in isotopic composition from positive to negative $\epsilon_{Nd}(0)$ signatures (Fig. 16). Although there are limited data, these do suggest that similar processes could have occurred in the development of the isotopic compositions of these three volcanoes. In marked contrast, the Sadiman lavas (Paslick *et al.* 1995; Zaitsev *et al.* 2019), although heterogeneous, form a near-linear mixing line suggesting derivation from two enriched distinct mantle sources.

Figure 17 shows that most of the Older Volcanics have compositions close to that of CHUR with Gelai and some examples from Essimingor and Loolmalasin having positive $\epsilon_{Nd}(0)$ signatures, whereas Kitumbeine and Tarosero have negative $\epsilon_{Nd}(0)$ signatures. Tarosero is distinct in exhibiting an extremely wide variation in $^{87}Sr/^{86}Sr$ ratios, suggesting significant crustal contamination or

https://doi.org/10.1017/S0016756822000619 Published online by Cambridge University Press

Table 6. Representative compositions of pyroxene in Mosonik phonolite

wt %	1	2	3	4	5	6
SiO_2	49.45	51.18	50.33	51.09	50.64	51.58
TiO_2	1.48	0.70	0.81	0.53	0.60	2.43
Al_2O_3	4.11	2.19	1.82	1.11	0.79	0.95
Fe_2O_3	3.40	4.77	5.10	7.06	10.80	26.74
FeO	6.75	9.10	10.83	12.30	12.58	1.31
MnO	n.d.	0.29	0.35	0.65	0.71	0.50
MgO	11.55	9.57	7.86	5.84	3.81	0.45
CaO	22.37	21.32	21.15	19.29	15.84	5.84
Na_2O	1.48	1.85	1.98	2.74	4.19	10.38
Total	100.59	100.97	100.23	100.61	99.95	100.18
Mol. %						
Cats	4.13	1.98	2.34	1.57	1.12	1.67
Tsch	3.15	2.34	1.19	0.14	–	–
Ae	9.49	13.52	14.76	20.95	32.69	82.68
Wo	40.82	40.90	41.79	39.89	33.59	12.02
Fs	10.47	14.35	17.41	20.28	21.16	2.26
En	31.94	26.90	22.52	17.17	11.43	1.38
Ternary mol. %						
Ae	9.68	13.57	15.60	21.86	33.40	91.91
Di	68.02	56.36	47.61	35.82	23.36	3.06
Hd	22.30	30.07	36.79	42.32	43.24	5.03

Cats = $CaTiAl_2O_6$; Tsch = $CaAl_2SiO_6$; Ae = $NaFe^{3+}Si_2O_6$; Wo = $Ca_2Si_2O_6$; Di = $CaMgSi_2O_6$; En = $Mg_2Si_2O_6$; Hd = $CaFe^{2+}Si_2O_6$. n.d. – not detected. FeO and Fe_2O_3 calculated from total FeO by assigning all Na_2O to $NaFe^{3+}Si_2O_6$.

mixing of ancient sources with diverse Rb/Sr ratios and uniform Sm/Nd ratios.

Figure 17 also includes new data for melilititic lavas of the Engaruka–Natron volcanic field. These lavas are distinct from most other Older and Younger Series volcanics in that they all have Nd isotopic compositions greater than CHUR (i.e. positive $\epsilon_{Nd}(0)$) and Sr isotopic compositions less than those of bulk earth, implying derivation from depleted mantle sources. Only the Gelai lavas, an Older Series volcanic, have a similar restricted range of isotopic compositions (Fig. 17).

8. Discussion

This work shows that Mosonik consists principally of diverse phonolitic nephelinites and phonolites as lavas and pyroclastic rocks. At the present level of exposure, lavas (or xenoliths) of silica-poor unevolved basaltic, basanitic, trachybasaltic, olivine nephelinite and nephelinite (*sensu stricto*) do not appear to be present. Hence, it is not possible to relate their petrogenesis to any of these compositions as a parental magma for the phonolitic nephelinite – phonolite suite. Zaitsev *et al.* (2015) and Sedova *et al.* (2018) have reported the presence of carbonatite and melilite-bearing nephelinite at Mosonik. These carbonatites might be small volume residual derivatives of carbonated silicate parental magmas as calcite is a common component of the groundmass of many of the nephelinitic lavas. With respect to carbonatite, Mosonik is similar to most other volcanoes of the Older Extrusive Series, all of which at the present levels of investigation, apart from Shombole, appear to lack significant volumes of carbonatite. This is in marked contrast to the Younger Series of volcanoes in which carbonatites are major components of the magmatism.

The melilite-bearing rocks, as is apparent from field observations, are volumetrically insignificant and thus cannot be parental to the voluminous phonolitic nephelinites and phonolites occurring at Mosonik. They might represent small volume melts formed during the initial stages of magmatism as indicated by the relatively unevolved pyroxene compositions reported by Sedova *et al.* (2018), which are similar to those in our Type 1 lavas.

The apparent absence of olivine nephelinite at Mosonik is important as such magmas are commonly considered as mantle-derived and parental to olivine-free nephelinites, phonolitic nephelinites and phonolites. The evolutionary trend for low-Mg moderately peralkaline (P.I. ~1.5) nephelinites, such as found at Mosonik, has been termed the 'Shombole trend' by Peterson (1989*a*,*b*), after the nephelinite–phonolite suite found at this eponymous volcano located geographically adjacent to Mosonik. Note that in this genetic scheme nephelinites are not derived by fractional crystallization of 'basaltic' sources (see below; Bell & Peterson, 1991).

The diversity of lava types at Mosonik indicates this is a polygenetic volcano with each phase of evolution characterized by repeated eruption of magmas of a similar type, but which differ in the details of their petrographic and mineralogical character. The changes in pyroxene (Fig. 10) and feldspar (Fig. 14) composition show that there is an overall trend of evolution from Type 1 through Type 2 to Type 3 magmatism. This trend might reflect fractionation of albite-rich alkali feldspar and diopsidic pyroxenes, resulting in the enrichment of residual liquids in potassium to an extent that potassium feldspar crystallizes as a groundmass phase.

The Mosonik lavas are characterized by high modal abundances of antecrysts and phenocrysts of clinopyroxene and nepheline (*c.* 30–60 vol. %) together with loosely bound crystal aggregates of pyroxene and nepheline derived from the disaggregation of ijolite xenoliths. The pyroxene assemblage is complex and consists of juxtaposed subhedral-to-euhedral mantled and broken crystals with intricate compositional zoning (Fig. 11). The overall assemblage is typical of crystallization of pyroxenes and nephelines under diverse non-equilibrium conditions followed by magma mixing. The presence of amphibole and garnet antecrysts (Figs 3b, 5b) which were not stable in their current Type 1 and 3 host lavas, also suggests their early crystallization as liquidus phases at higher pressures followed by transport, reaction and magma mixing. Accordingly, the antecryst and phenocryst assemblage is considered to be a non-equilibrium rheologically concentrated assemblage transported by a magma which subsequently crystallized more evolved groundmass sodic pyroxenes, nepheline and alkali feldspar.

Recent hypotheses for the emplacement of magmas in small volume sub-volcanic environments have proposed that large continuously fractionating magma chambers do not exist (Emeleus & Troll, 2014; Floess *et al.* 2019; Hepworth *et al.* 2020; Savard & Mitchell, 2021). Following these concepts, the mineralogical variations of the Type 1–3 lavas can be explained by fractional

https://doi.org/10.1017/S0016756822000619 Published online by Cambridge University Press

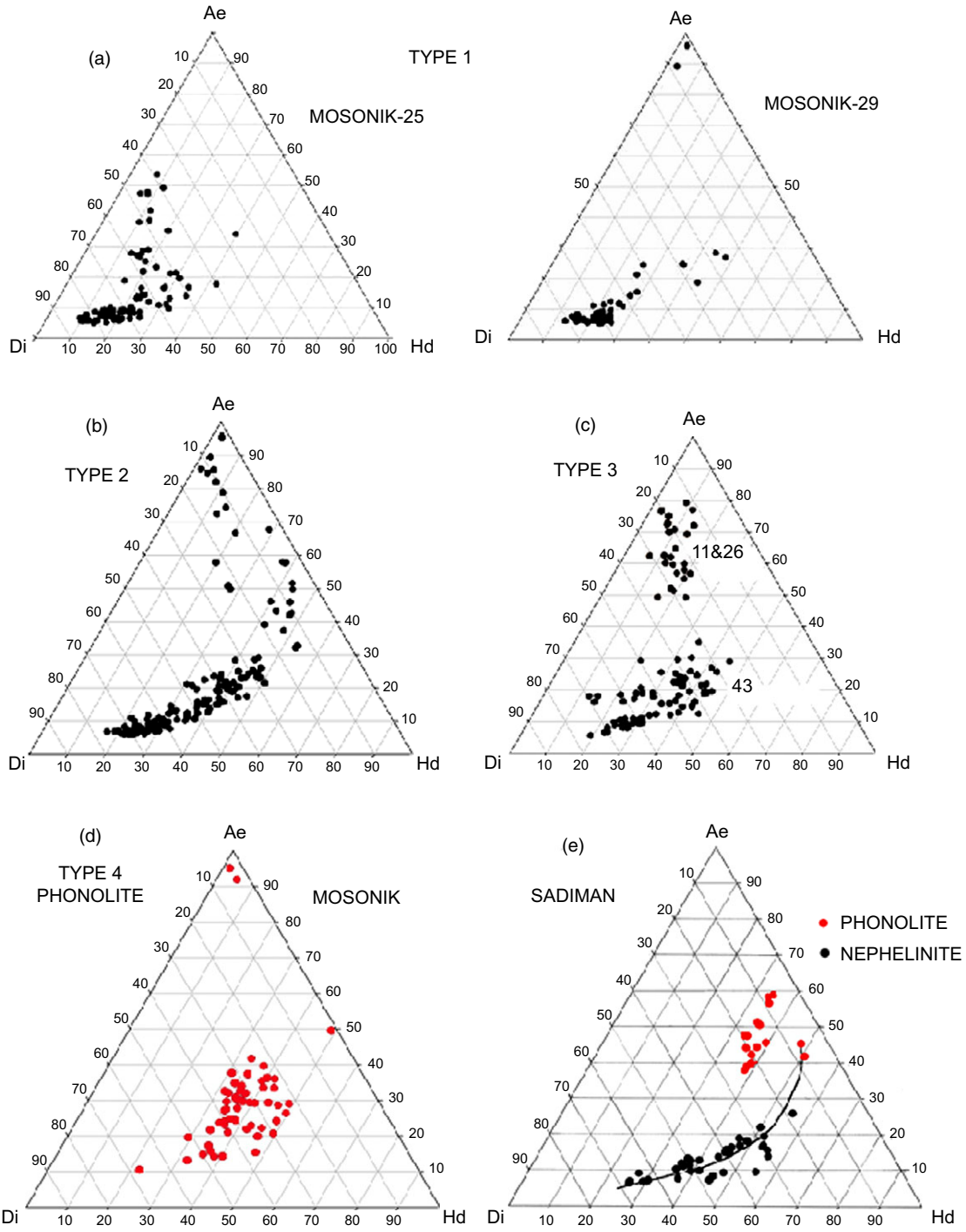

Fig. 10. (Colour online) Composition (mol. %) of clinopyroxenes in representative Mosonik lavas expressed in terms of the diopside–hedenbergite–aegirine (Di–Hd–Ae) ternary system: (a) Type 1 nephelinites; (b) Type 2 and 3 nephelinites; (c) Type 4 phonolites; (d) nephelinites and phonolites from Sadiman volcano (Zaitsev *et al.* 2012).

crystallization of many individual batches of magmas derived from a common source coupled with magma mixing as a result of intrusion of magma into crystal-melt mushes and/or entrainment of crystals derived from disaggregation of pre-existing fully crystallized melts; i.e. members of the ijolite suite. *From these observations it is apparent that none of the bulk compositions of the Mosonik lavas represent those of a liquid and that their compositions cannot be used usefully for any geochemical modelling of crystal fractionation schemes* (see below).

The relationships of the phonolites to the less-evolved lavas cannot be one of simple fractional crystallization and a continuation of an evolutionary trend from Type 1 to Type 2 and 3 nephelinite lavas as suggested by clinopyroxene compositions, and thus there is no mineralogical/petrographic continuum between the

https://doi.org/10.1017/S0016756822000619 Published online by Cambridge University Press

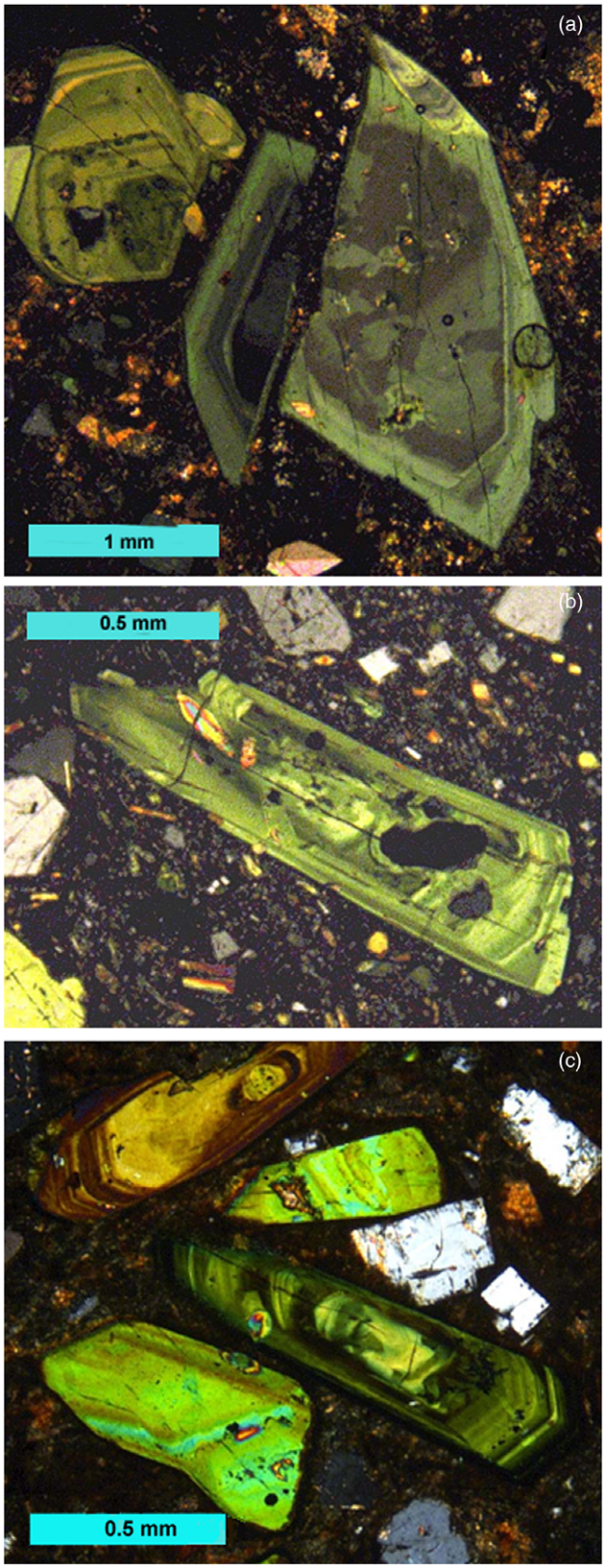

Fig. 11. (Colour online) Photomicrographs illustrating the complex compositional zoning of euhedral and anhedral phenocrystal clinopyroxenes in (a, b) Type 2 and (c) Type 3 Mosonik lavas. The juxtaposition of clinopyroxenes of diverse character are considered to indicate magma mixing.

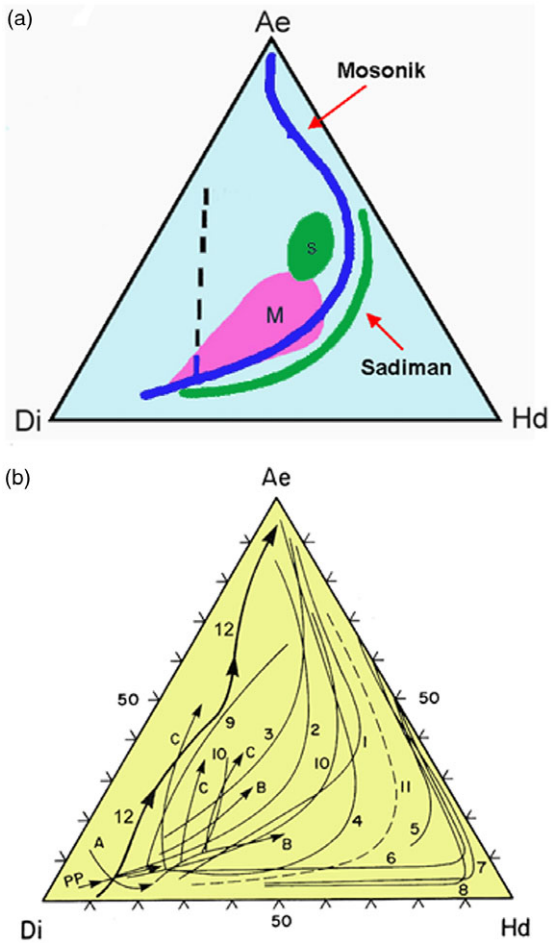

Fig. 12. (Colour online) (a) Compositional trends of clinopyroxenes in types 1–3 phonolitic nephelinites from Mosonik (blue curve; this work) and nephelinites from Sadiman (green curve; Zaitsev *et al*. 2012). Dashed black line shows the trend of compositions in MOS25 (see Fig. 10). Also shown are compositional fields for clinopyroxenes in phonolites from Mosonik (M; this work) and Sadiman (S; Zaitsev *et al*. 2012). (b) Compositional trends for clinopyroxenes in a variety of alkaline volcanic and plutonic rocks (after Mitchell & Vladykin, 1996) for comparison with those of Mosonik and Sadiman lavas: 1 – Morotu; 2 – Uganda; 3 – Itapirapua; 4 – South Qoroq; 5 – pantellerite; 6 – Nandewar; 7 – Ilimausaq; 8 – Coldwell ferroaugite syenite; 9 – Turja; 10 – Iron Hill; 11 – Coldwell nepheline syenite; 12 – Little Murun complex; A, B, C – Fen complex (data sources in Mitchell & Platt, 1982; Mitchell & Vladykin, 1996). The Mosonik and Sadiman pyroxene compositional trends approximate those of the mildly peralkaline Ugandan volcanics (trends 1 and 2) with intermediate oxygen fugacities.

phonolites and the less-evolved magmas. Thus, Figure 10 shows the majority of pyroxene compositions in the phonolites do not exceed 30 mol. % Ae, and Figure 14 shows that they contain albite-rich alkali phenocrysts and groundmass potassium feldspars with a wide range in compositions which are very similar to feldspars occurring in Type 1 lavas. These observations suggest that the phonolites have a closer relationship to Type 1 lavas rather than the more evolved Type 2 and 3 lavas; and this in turn implies that the phonolites are not simple fractionation derivatives of the latter.

A detailed discussion of the genesis of the Mosonik phonolites is considered to be premature and beyond the scope of this preliminary investigation of the volcano. However, their origins cannot be compared usefully with hypotheses suggested for some other

https://doi.org/10.1017/S0016756822000619 Published online by Cambridge University Press

Table 7. Representative compositions of garnet in Type 3 nephelinite lavas

wt %	1c	2r	3c	4r	5c	6r	7c	8r
SiO_2	30.16	32.01	28.05	29.62	29.31	29.28	29.92	29.61
TiO_2	13.32	9.90	15.73	13.90	17.62	15.35	17.49	15.65
Al_2O_3	0.40	0.61	1.36	0.36	0.42	0.39	0.33	0.51
Fe_2O_3	17.24	19.40	16.92	18.08	11.66	16.04	10.50	14.19
FeO	5.66	5.39	5.00	5.91	9.50	6.74	10.42	7.81
MgO	0.64	0.43	1.00	0.59	0.50	0.55	0.33	0.37
CaO	32.19	32.02	31.93	31.97	31.42	31.85	31.30	31.80
Total	99.67	99.76	99.94	100.43	100.43	100.20	100.29	99.94
Mol. % end-members								
Slo	19.38	11.02	23.96	22.40	24.43	23.57	21.18	21.19
Slo-Al	2.01	3.05	6.81	1.80	2.10	1.96	1.65	2.56
Mmt	40.37	34.97	35.55	40.41	59.74	45.60	63.34	50.94
Mmt-Mg	2.28	–	–	–	–	–	–	–
Adr	34.00	47.99	27.11	32.37	10.04	25.95	8.86	22.15
Skg	–	1.10	–	0.52	2.58	0.80	3.55	1.59
Khh	1.94	1.81	3.05	2.49	1.22	1.28	–	0.59
Ternary mol. %								
Slo	21.82	14.54	32.93	24.95	26.78	26.15	24.02	24.52
Mmt	43.51	36.02	38.05	41.67	62.88	47.07	66.65	52.60
Adr	34.68	49.44	29.02	33.38	10.54	26.78	9.33	22.88

FeO and Fe_2O_3 calculated on the basis of 8 cations and 12 oxygens following Droop (1987). Garnet end-members calculated using Locock (2008). c – core; r – rim. Slo = schlorlomite ($Ca_3Ti_2(SiFe^{3+}{}_2)O_{12}$); Slo-Al = schlorlomite-Al ($Ca_3Ti_2(SiAl_2)O_{12}$); Mmt = morimotoite ($Ca_3(TiFe^{2+})Si_3O_{12}$); Mmt-Mg = morimotoite-Mg ($Ca_3(TiMg)Si_3O_{12}$); Adr = andradite ($Ca_3Fe^{3+}{}_2Si_3O_{12}$); Skg = skiagite $Fe^{2+}{}_3Fe^{3+}{}_2Si_3O_{12}$; Khh = khoharite $Mg_3Fe^{3+}{}_2Si_3O_{12}$

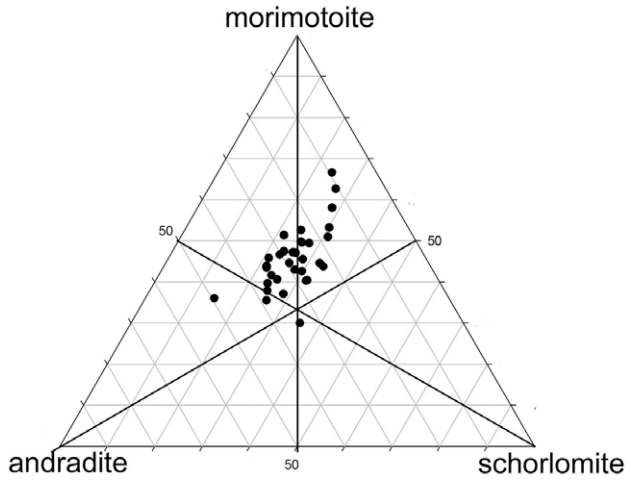

Fig. 13. Compositions (mol. %) of garnets in Type 3 phonolitic nephelinites from Mosonik.

examples of consanguineous nephelinite–phonolite volcanism such as is found in Tenerife (Ablay *et al.* 1998; Bryan *et al.* 2002) and Saghro (Berger *et al.* 2009), where phonolites are considered to form as a consequence of fractional crystallization of unevolved basaltic or basanitic rocks which are abundant and characteristic of these occurrences. In contrast, the Freemans Cove basanite–nephelinite suite is considered by Mitchell & Platt (1984) to be a partial melting sequence with phonolites formed during low-pressure fractional crystallization of evolved nephelinite.

Comparisons with other members of the Older Extrusive Series volcanic suites with Mosonik lavas are difficult as detailed petrographic and mineralogical studies of these volcanoes are lacking, and they have been classified by Paslick *et al.* (1995, 1996) and Mana *et al.* (2012, 2015) using the IUGS TAS diagram and not on the basis of the actual mineralogy. As noted in Section 5 above, the IUGS system incorrectly classifies many crystal-phyric alkaline lavas as plagioclase-bearing rocks, i.e. phonotephrite or basanite. Regardless, it is apparent that the Gelai and Shombole volcanoes which are geographically closest to Mosonik appear to be similar in that they consist principally of phonolitic nephelinites and phonolites (Peterson, 1989*a*,*b*; Paslick *et al.* 1996; Dawson, 2008; Mana *et al.* 2015). However, Gelai and the nearby Ketumbeine volcano also contain basal suites of basaltic lavas which might, or might not, be related to the undersaturated lavas as it is not known if these volcanoes were merely erupted onto a pre-existing basaltic substrate. With respect to the relationships of the nephelinite–phonolite suites, Tarosero although characterized by the presence of eudialyte-bearing alkaline-to-peralkaline trachytes and quartz, is

https://doi.org/10.1017/S0016756822000619 Published online by Cambridge University Press

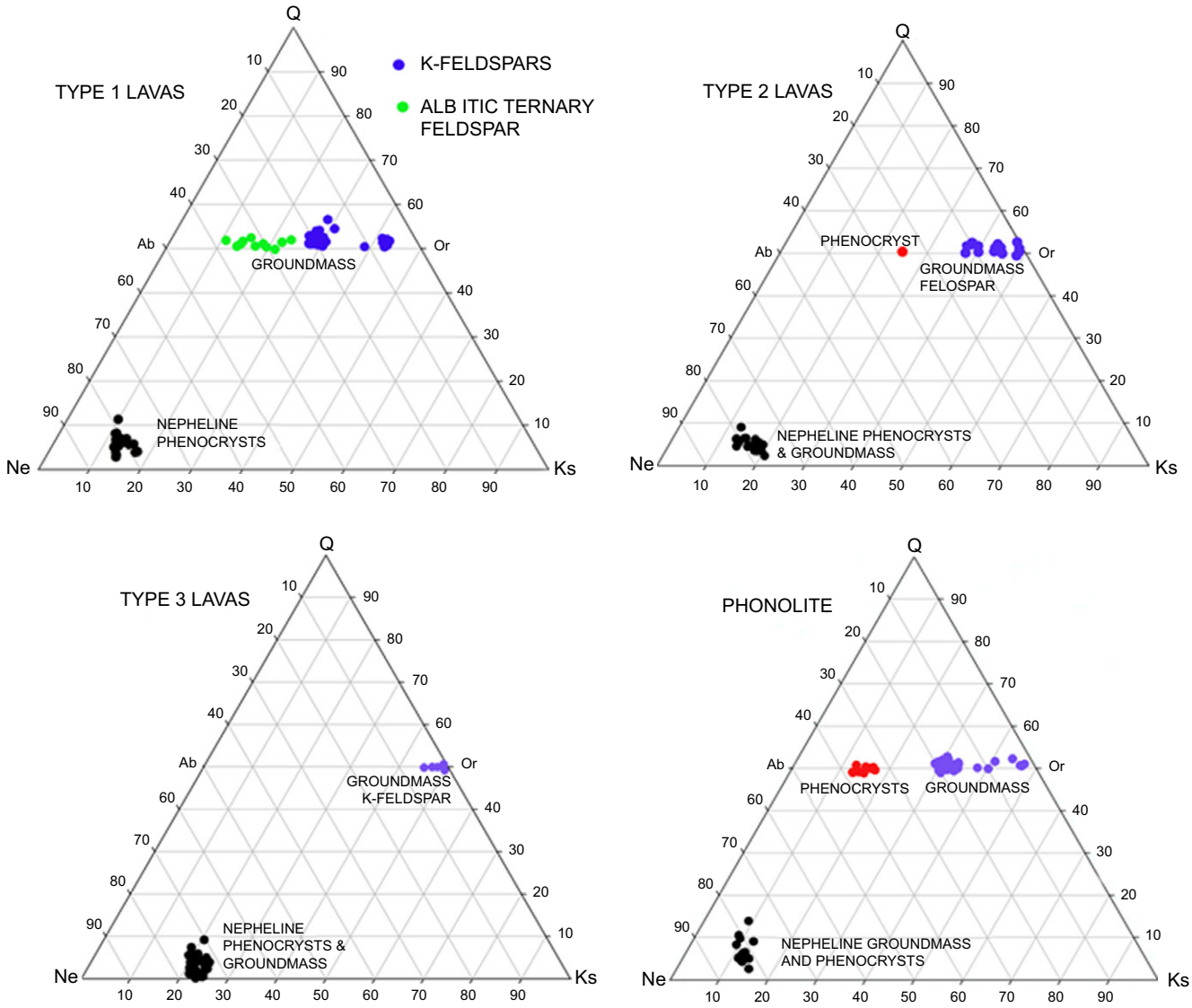

Fig. 14. (Colour online) Compositions (wt % end-members) of nepheline and feldspar for Mosonik lavas expressed in the quartz–nepheline–kalsilite ternary system (Q–Ne–Ks). Ab – albite; Or – $KAlSi_3O_8$ (orthoclase).

situated upon an pre-existing extensive alkali basalt-benmoreite plateau. There is no obvious geological or genetic relationship of this basaltic plateau to the Tarosero trachytes (Dawson, 2008), and a recent study by Braunger *et al.* (2021) has concluded that the peralkaline rocks cannot be derived by fractional crystallization of such basaltic parents.

Because of the absence of unevolved lavas at Mosonik, and the observation that none of the lavas represent liquid compositions, it is not possible to identify a possible parental magma for even the least evolved Type 1 lavas. These lavas contain the least evolved pyroxene compositions and are thus similar to pyroxenes in diverse unevolved nephelinites. This, and the presence of ijolite xenoliths, indicates a parental magma of broadly nephelinitic composition, and a typical sodic nephelinite parental magma might be considered as a potential parent for these and small volumes of melilitite-bearing nephelinite. A melilite nephelinite parent, such as suggested for the Hanang nephelinite volcanism (Baudouin *et al.* 2016), is precluded by the absence of significant volumes of such lavas at Mosonik. However, further speculation as to the actual composition of any parental magma is not especially desirable as there is as yet no evidence from Mosonik which could be used to predict its composition or, whether or not, it might be olivine-bearing.

As the northern Tanzania volcanoes were erupted through old cratonic lithosphere overlain by no more than a thin veneer of mobile-belt rocks, there is potential for significant crustal contamination of the magmas during their ascent (Dawson, 2008). However, extensive contamination by high silica crust is not reflected in the mineralogy or major-element composition of the volcanic rocks, as they are demonstrably silica-undersaturated and minerals indicative of contamination are absent. However, minor contamination might be reflected in their trace-element

https://doi.org/10.1017/S0016756822000619 Published online by Cambridge University Press

Table 8. Representative compositions of nepheline

wt %	1	2	3	4	5	6	7	8
SiO_2	44.09	43.19	43.73	42.65	43.51	43.90	43.97	43.02
Al_2O_3	32.73	31.83	32.00	31.98	30.10	29.78	33.24	33.58
Fe_2O_3	0.72	1.82	2.40	1.85	3.03	3.69	0.56	0.73
Na_2O	17.16	16.44	16.84	16.68	16.49	16.31	18.05	17.92
K_2O	4.83	5.94	5.92	6.92	6.50	6.29	3.72	4.82
Total	99.53	99.22	100.80	100.08	99.64	99.97	99.54	100.07
Structural formulae on the basis of 32 oxygens								
Si	8.425	8.322	8.289	7.992	8.134	8.284	8.394	8.149
Al	7.575	7.768	7.711	8.008	7.866	7.716	7.606	7.851
Fe^{3+}	0.104	0.267	0.346	0.271	0.447	0.540	0.081	0.106
Na	6.392	6.203	6.262	6.291	6.246	6.154	6.698	6.671
K	1.184	1.475	1.449	1.717	1.620	1.562	0.908	1.181
□	0.425	0.322	0.289	0.008	0.134	0.284	0.394	0.149
Mol. % end-members								
FeNe	1.30	3.31	4.30	3.32	5.46	6.65	1.01	1.31
Ks	14.76	18.34	18.00	21.07	19.80	19.21	11.34	14.66
Ne	78.37	73.83	73.50	73.85	70.87	69.06	82.61	81.50
Q	5.57	4.52	4.20	1.77	3.87	5.09	5.05	2.53

Composition: (1) phenocryst Type 1 nephelinite; (2 and 3) phenocryst and groundmass, Type 2 nephelinite; (4 and 5) phenocryst core and rim, Type 3; (6) groundmass Type 3 nephelinite; (7 and 8) phenocryst and groundmass, phonolites. *Ks* = $KAlSiO_4$; *Ne* = $NaAlSiO_4$; *FeNe* = $NaFe^{3+}SiO_4$; *Q* = excess SiO_2; □ = cation vacancies calculated after Mitchell (1972).

and isotopic compositions, as noted in Section 5 above for the heavy REEs.

Previous studies by Paslick *et al.* (1995, 1996) and Mana *et al.* (2012, 2015) have attempted to explain the observed geochemistry of the Older Extrusive Series using assimilation–fractional crystallization (AFC) models which incorporate potential mantle and crustal contaminants. Paslick *et al.* (1995) suggested that the trace-element and isotopic Sr, Nd and Pb isotopic characteristics of the Tanzanian eruptive rocks could originate from underplating of the craton by an oceanic island basaltic asthenospheric melt which became isolated for *c.* 2 Ga, thus forming an enriched lithospheric mantle which was subsequently remelted and metasomatized during rifting by the mantle plume presently located under the Tanzania Craton (Weeraratne *et al.* 2003). An assessment of contamination by crustal material was essentially inconclusive, as the compositions of potential contaminants or mechanisms of contamination are not actually known. However, crustal contamination for some of the rocks analysed was not entirely discounted. Subsequently, Paslick *et al.* (1995) suggested that 'indirect' crystal contamination occurred in northern Tanzania by crustal granulites and that the rocks analysed contain 'xenocrysts' derived from such rocks incorporated into earlier batches of magma. However, Paslick *et al.* (1996) failed to recognize the petrological complexity of the nephelinites and that many of the supposed 'xenocrysts', especially the common complexly zoned pyroxenes, are actually consanguineous antecrysts (see above). Thus, the conclusions regarding 'indirect' crustal contamination are unfounded and the modelling using hypothetical granulite compositions is invalid.

Mana *et al.* (2015) also determined that northern Tanzanian volcanic rocks exhibit a very wide range in their Sr–Nd–Pb isotopic compositions. Figure 17 shows that these data, apart from Tarosero, define a heterogeneous negative Sr–Nd trend from the East African Carbonatite Line towards enriched mantle EM1 for lavas of the Older Extrusive Series. Mana *et al.* (2015) determined that $^{87}Sr/^{86}Sr$ ratios increase and Ce/Pb ratios decrease with increasing bulk-rock SiO_2, a correlation not found for the Mosonik lavas analysed in this work, and also noted that, at best, only limited evidence for crustal assimilation could be recognized. Geochemical modelling using AFC models incorporating isotopic and trace-element data for crustal xenoliths by Paslick *et al.* (1995) and Mana *et al.* (2012, 2015) have failed to explain the observed geochemistry of the northern Tanzanian lavas, a conclusion which is not surprising given that none of the lavas analysed represent liquid compositions coupled with the expected heterogeneity of the crust in this region and the unknown compositions of potential contaminants. Consequently, we have not attempted to apply any geochemical modelling to the genesis of the Mosonik lavas as we consider that this would make no advance on the inconclusive observations of Paslick *et al.* (1995, 1996) or Mana *et al.* (2012, 2015). However, in common with Paslick *et al.* (1995) and Mana *et al.* (2012, 2015), we consider that partial melting of ancient metasomatized lithospheric mantle is a possible source for these lavas.

https://doi.org/10.1017/S0016756822000619 Published online by Cambridge University Press

Table 9. Representative compositions of groundmass feldspar in Type 1 nephelinite lavas

wt %	1	2	3	4	5	6
SiO_2	63.28	63.14	63.49	64.74	63.03	63.23
Al_2O_3	21.47	21.08	18.63	18.49	18.21	19.01
Fe_2O_3	0.85	0.46	3.25	0.99	2.16	1.41
CaO	1.19	1.19	–	–	–	–
Na_2O	6.86	7.83	4.28	4.71	2.25	1.67
K_2O	4.83	4.44	8.72	9.76	13.67	13.84
BaO	1.31	0.64	1.44	0.49	1.35	1.45
Total	99.79	98.78	99.81	99.18	100.67	100.61
Structural formulae on the basis of 32 oxygens						
Si	11.442	11.580	11.686	11.888	11.719	11.718
Al	4.575	4.416	4.041	4.002	0.990	4.152
Fe^{3+}	0.116	0.062	0.450	0.137	0.302	0.197
Ca	0.231	0.227	–	–	–	–
Na	2.405	2.649	1.527	1.677	0.811	0.600
K	1.074	1.007	2.048	2.286	3.243	3.272
Ba	0.093	0.045	0.104	0.035	0.098	0.105
Mol. % end-members						
Cs	2.42	1.12	2.82	0.88	2.37	2.65
An	6.01	5.70	–	–	–	–
FeOr	3.02	1.55	12.24	3.42	7.28	4.94
Ab	62.75	67.86	41.52	41.94	19.54	15.09
Or	28.85	23.77	43.42	53.76	70.82	77.32
Ternary feldspars (mol. %)						
An	6.36	5.86	–	–	–	–
Ab	66.31	69.72	48.88	43.82	21.62	16.33
Or	27.31	24.42	51.12	56.18	78.38	83.67

Compositions: (1 and 2) M23; (3 and 4) M31; (5 and 6) M25. Cs = $BaAl_2Si_2O_8$; An = $CaAl_2Si_2O_8$; Ab = $NaAlSi_3O_8$; FeOr = $KFeSi_3O_8$; Or = $KAlSi_3O_8$. Total Fe expressed as Fe_2O_3

For comparative purposes, Sr–Nd isotopic data obtained in this work (Fig. 17; Table 15) are given for Younger Extrusive Series lavas from the Oldoinyo Lengai Nasira combeite wollastonite nephelinite parasitic cones (Mitchell, 2009), Oldoinyo Lengai 2007 ash (Mitchell & Dawson, 2007) and Recent (*c.* 434–166 ka; this work) melilitites of the Natron–Enkaruka volcanic field (Dawson & Powell, 1969). The datum for the Oldoinyo Lengai ash ($\epsilon_{Nd}(0)$ +0.1) is similar to previous studies of the lavas (Bell & Dawson, 1995) with $\epsilon_{Nd}(0)$ +0.1 to +0.48, although the Nasira lavas have $\epsilon_{Nd}(0)$ +0.1 to +0.4 and slightly lower $^{87}Sr/^{86}Sr$ ratios (Table 15). These compositions plot essentially along the East African Carbonatite Line of Bell & Blenkinsop (1987), which is interpreted to indicate derivation from mantle sources with the variation in isotopic composition due to mixing of different proportions of two mantle end-members. One is postulated to have a composition similar to that of bulk earth (EM1) and the other a depleted source with higher Sm/Nd and lower Rb/Sr ratios (HIMU).

In contrast to Oldoinyo Lengai, the Engaruka–Natron melilitites have Sr–Nd isotopic compositions ($\epsilon_{Nd}(0)$ +2.3 to 4.7) that form an array extending from, and above, the East African Carbonatite Line (Fig. 17). These data support those obtained for three Engaruka melilitites ($\epsilon_{Nd}(0)$ +2.4 to 2.64) by Keller *et al.* (2006). If the isotopic compositions of the melilitites are also derived by mixing between two mantle sources, these data might imply a greater contribution of the depleted end-member than is present in the source of the Oldoinyo Lengai lavas and no genetic relationship to Oldoinyo Lengai silicate lavas. We contend also, on the basis of these data, that the Dorobo melilitite cone (Keller *et al.* 2006) has merely a geographic intrusive relationship to lavas on the lower slopes of the Oldoinyo Lengai cone and is a part of the Recent Natron–Engaruka suite.

Of importance with regards to the Younger Extrusive Series lavas is that there is no isotopic or mineralogical evidence for any crustal contamination, and they do not exhibit the heterogeneous isotopic signatures and negative $\epsilon_{Nd}(0)$ values

https://doi.org/10.1017/S0016756822000619 Published online by Cambridge University Press

Table 10. Representative compositions of feldspar in Type 2 and 3 nephelinites and phonolite lavas

wt %	1	2	3	4	5	6	7	8	9	10
SiO_2	63.51	64.57	64.27	64.87	63.37	66.83	66.11	65.18	64.07	65.21
Al_2O_3	16.55	17.71	18.07	17.50	17.81	20.24	19.77	18.94	18.35	17.57
Fe_2O_3	4.25	1.61	1.47	1.36	0.90	0.19	0.35	0.77	0.44	0.69
Na_2O	1.08	0.81	3.11	2.46	1.24	8.35	7.86	4.11	2.89	1.08
K_2O	12.52	14.82	12.04	13.06	14.93	4.46	4.76	10.98	12.60	14.69
BaO	1.53	0.92	0.78	0.50	0.82	0.36	0.60	0.30	0.50	0.22
Total	99.44	100.44	99.74	99.75	99.07	100.43	99.45	100.28	98.85	99.46
Structural formulae on the basis of 32 oxygens										
Si	11.906	11.953	11.878	11.991	11.909	11.833	11.855	11.863	11.913	12.079
Al	3.656	3.864	3.936	3.812	3.945	4.224	4.178	4.063	4.021	3.836
Fe^{3+}	0.600	0.224	0.204	0.189	0.127	0.025	0.047	0.106	0.062	0.096
Na	0.393	0.291	1.124	0.882	0.452	2.866	2.733	1.450	1.042	0.388
K	2.994	3.599	2.839	3.080	3.579	1.007	1.089	2.550	2.989	3.471
Ba	0.112	0.067	0.057	0.036	0.060	0.025	0.042	0.021	0.036	0.016
Mol. % end-members										
Cs	3.21	1.73	1.41	0.91	1.48	0.64	1.09	0.53	0.90	0.41
FeOr	17.13	5.81	5.10	4.73	3.11	0.65	1.22	2.62	1.51	2.48
Ab	11.22	7.54	27.79	22.05	11.04	73.52	70.73	36.07	25.62	10.01
Or	68.44	84.92	65.70	72.31	84.37	25.19	26.96	60.76	71.97	87.10
Ternary feldspars (mol. %)										
Ab	14.08	8.15	29.73	23.37	11.57	74.48	72.40	37.24	26.25	10.31
Or	85.92	91.85	70.27	76.63	88.43	25.52	27.60	62.76	73.75	89.69

Compositions: (1 and 2) Type 2 M7; (3 and 4) Type 2 M10; (5) Type 3 M748; (6 and 7) Type 4 phenocrysts phonolite; (8–10) Type 4 groundmass phonolite. Cs = $BaAl_2Si_2O_8$; Ab = $NaAlSi_3O_8$; FeOr = $KFeSi_3O_8$; Or = $KAlSi_3O_8$. Total Fe expressed as Fe_2O_3

Table 11. Representative compositions of ulvöspinel-magnetite in Type 1 nephelinite lavas

wt %	1	2	3	4	5	6	7	8	9	10
TiO_2	17.00	18.09	18.90	20.38	16.70	17.25	16.26	17.04	17.33	17.27
Al_2O_3	0.21	0.47	0.24	0.48	2.98	2.60	2.81	3.00	0.29	0.81
FeO	44.56	45.52	46.41	47.60	41.82	44.39	41.82	42.55	45.43	45.54
Fe_2O_3	36.67	33.47	32.51	28.84	33.48	31.90	36.25	33.32	34.25	34.38
MnO	2.08	2.00	2.17	2.00	0.77	0.76	0.70	0.84	1.03	0.96
MgO	0.31	n.d.	n.d.	n.d.	2.58	1.15	2.81	2.44	0.17	0.33
Total	100.83	99.55	100.23	99.30	98.52	98.05	100.65	99.19	98.50	99.29
Mol % end-members										
$MgAl_2O_4$	0.31	–	–	–	4.45	3.93	4.09	4.44	0.44	1.21
Mg_2TiO_4	0.63	–	–	–	3.97	0.35	4.69	3.52	0.16	0.03
Mn_2TiO_4	3.30	3.24	3.48	3.24	1.24	1.25	1.10	1.34	1.68	1.55
Fe_2TiO_4	44.01	48.78	50.28	55.31	42.50	48.32	39.54	43.44	48.23	47.91
Fe_3O_4	51.75	48.00	46.25	41.49	47.85	46.17	50.57	47.26	49.50	49.30

Compositions: (1 and 2) core and rim M25; (3 and 4) core and rim M25; (5 and 6) core and rim M31; (7 and 8) core and rim M31; (9 and 10) single crystals M18. n.d. – not detected. FeO and Fe_2O_3 calculated from stoichiometry (Droop, 1987).

https://doi.org/10.1017/S0016756822000619 Published online by Cambridge University Press

Table 12. Representative compositions of magnesio-hastingsite

wt %	1	2			1	2
SiO_2	41.85	40.25	T-site	Si	6.189	6.089
TiO_2	3.58	3.48		Al	1.811	1.911
Al_2O_3	10.85	10.93	C-site	Al	0.080	0.025
FeO_T	12.68	16.05		Ti	0.399	0.393
MnO	n.d.	0.21		Fe^{3+}	0.127	0.224
MgO	13.40	11.32		Fe^{2+}	1.441	1.794
CaO	11.33	11.62		Mn	–	0.027
Na_2O	3.41	3.14		Mg	2.954	2.537
K_2O	1.27	1.13	B-site	Ca	1.795	1.872
Total	98.42	98.13		Na	0.205	0.128
Recalculated Fe			A-site	Na	0.773	0.787
FeO	11.65	14.27		K	0.240	0.217
Fe_2O_3	1.14	1.98				
Total	98.48	98.58				
Mg no.	0.67	0.59				

FeO_T – total Fe calculated as FeO; FeO and Fe_2O_3 are calculated using the method of Droop (1987). n.d. – not detected.

Table 13. Representative compositions of barytolamprophyllite

wt %	1	2	SF	1	2
SiO_2	29.97	30.35	Si	3.830	3.876
TiO_2	26.33	25.47	Ti	2.530	2.446
FeO_T	4.01	4.81	Fe	0.429	0.514
MnO	0.55	0.68	Mn	0.060	0.074
CaO	1.69	1.84	Ca	0.231	0.252
SrO	3.67	3.28	Sr	0.272	0.243
BaO	22.39	21.79	Ba	1.121	1.091
Na_2O	8.50	8.38	Na	2.106	2.075
K_2O	1.40	1.79	K	0.228	0.292
	98.51	98.39			

FeO_T – total Fe as FeO; SF – structural formula calculated on the basis of 16 atoms of oxygen.

characteristic of the Older Extrusives. This observation cannot be fortuitous and suggests that the Younger Extrusives did not interact with crustal material and the Oldoinyo Lengai and Engaruka magmas are each derived from different sources, the former originating from ancient metasomatized lithosphere with partial melting stimulated by introduction of asthenospheric material derived from the currently rising sub-cratonic plume. In contrast, the Natron–Engaruka continental melilitites might be direct partial melts of asthenospheric material with no lithospheric mantle contributions (Brey, 1978; Rogers *et al.* 1992; Mattsson *et al.* 2013). Although further discussion of the genesis of these lavas is beyond the scope of this work, the isotopic characteristics of the Older

Table 14. Composition of peralkaline glass inclusions in nepheline

wt %	1	2	3	4	5	6
SiO_2	49.04	51.91	50.51	46.24	48.29	51.96
TiO_2	1.11	0.45	1.50	1.56	1.50	1.10
Al_2O_3	2.26	4.98	2.83	2.32	2.92	3.70
FeO_T	12.31	14.13	13.45	12.68	13.19	16.75
MnO	0.47	0.70	0.39	0.40	0.44	0.77
MgO	0.36	0.61	0.50	0.63	0.59	0.66
CaO	8.11	4.49	4.90	10.72	11.05	3.19
Na_2O	16.07	15.91	16.90	16.85	17.00	15.32
K_2O	3.44	4.57	4.16	3.01	3.18	4.50
Cl	0.51	0.44	0.52	0.42	0.51	0.45
SO_3	0.73	0.52	1.02	0.84	0.93	0.52
Γ	94.41	98.71	96.68	95.67	99.60	98.92
P.I.	12.78	6.25	11.41	13.35	10.76	8.13

P.I. – peralkalinity index molar $(Na_2O + K_2O)/Al_2O_3$

versus the Younger Series lavas indicates a distinct change in the source character with the temporal development of the rift, and that at least three distinct petrogenetic processes have played a role in the genesis of the lavas of the North Tanzanian Divergence.

9. Summary and conclusions

This investigation has shown that Mosonik, a deeply dissected polygenetic Older Extrusive Series volcano, is composed principally of diverse phonolitic nephelinite and phonolite lavas, with minor amounts of melilite-bearing nephelinite and carbonatite. Less-evolved olivine nephelinites (*sensu stricto*), peralkaline nephelinites and basalts are not present at the current level of exposure. At least three types of phonolitic nephelinite are present and distinguished on the presence or absence of amphibole or garnet antecrysts and differing populations of complexly zoned clinopyroxenes. The phenocryst assemblage is typical of hybrid lavas derived from magma mixing. As a consequence of the high modal proportions of clinopyroxene and nepheline phenocrysts and the hybrid character of the lavas, their bulk compositions do not represent those of the liquids from which they crystallized and an unevolved parental magna cannot be defined. This observation renders AFC modelling of major and trace elements as inappropriate. Isotopic data for Mosonik are similar to those previously determined for other Older Extrusive Series rocks. Interpretation of these data is ambiguous and the observed isotopic heterogeneity might reflect mixing of Sr and Nd derived from two distinct mantle sources with or without lower crustal granulite contamination.

It is also proposed that three distinct mantle sources might have contributed to the isotopic character of the Older and Younger Extrusives. The Older Extrusives might be derived by partial melting of ancient metasomatized lithospheric mantle with mixing of Sr and Nd from two sources coupled with minor lower crustal

https://doi.org/10.1017/S0016756822000619 Published online by Cambridge University Press

Table 15. Isotopic composition of Mosonik, Oldoinyo Lengai and Engaruka volcanic rocks

Sample	$^{143}Nd/^{144}Nd$	2Φ	ϵNd	$^{87}Sr/^{86}Sr$	2Φ	Type
Mosonik						
MOS7	0.512459	0.000007	−3.5	0.704904	0.000021	2
MOS8	0.512213	0.000007	−8.3	0.704217	0.000018	1
MOS26	0.512479	0.000008	−3.1	0.704814	0.000017	3
MOS28	0.512216	0.000008	−8.2	0.704978	0.000017	1
MOS29	0.512373	0.000006	−5.2	0.705011	0.000019	2
MOS35	0.512257	0.000006	−7.4	0.704672	0.000019	4
MOS36	0.512244	0.000008	−7.7	0.704543	0.000017	4
MOS43	0.512440	0.000007	−3.9	0.704781	0.000016	3
Oldoinyo Lengai						
Lengai	0.512641	0.000007	0.1	0.704357	0.000010	carb
NC-2	0.512641	0.000007	0.1	0.704177	0.000010	cwn
NC-3	0.512647	0.000007	0.2	0.704204	0.000009	cwn
SC	0.512657	0.000007	0.4	0.704202	0.000010	cwn
Natron–Engaruka						
HMC1	0.512822	0.000007	3.6	0.703756	0.000010	mel
HILL3	0.512834	0.000007	3.8	0.703832	0.000010	mel
AH	0.512878	0.000010	4.7	0.703691	0.000010	mel
KS	0.512759	0.000011	2.4	0.703916	0.000009	mel
HILL5	0.512754	0.000006	2.3	0.703740	0.000009	mel
BH	0.512886	0.000009	4.8	0.703374	0.000010	mel
HILL12	0.512852	0.000007	4.2	0.703634	0.000010	mel
DEETI	0.512762	0.000006	2.4	0.703636	0.000009	mel
BD-108	0.512767	0.000008	2.5	0.703604	0.000008	mel
Mosonik measured standard values (U of Alberta)						
JNdi-1	0.512101	0.000011 (n = 44)				
NBS 987	0.710265	0.000036 (n = 4)				
Lengai–Natron–Engaruka measured standard values (Memorial University)						
JNdi-1	0.512115	0.000009 (n = 26)				
NBS 987	0.710240	0.000014 (n = 20)				

Accepted values of the standards JNdi-1 and NBS 987 are $^{143}Nd/^{144}Nd = 0.512107$ and $^{87}Sr/^{86}Sr = 0.710240$, respectively. Mosonik lavas (types 1–4) were analysed at the University of Alberta (see online Supplementary Material). Oldoinyo Lengai 2007 silicate ash, combeite wollastonite nephelinites (cwn) from North and South Nasira parasitic cones (NC and SC) and Engaruka melilitites (mel) were analysed at Memorial University of Newfoundland (see online Supplementary Material). HMC – Half Moon Crater; AH – Amykron Hill; KS – Kisete; BH – Baboon Hill; BD-108 – Lalarasi.

contamination. Partial melting was undoubtedly induced by the plume currently impinging on the Tanzanian craton, and represents the initial interaction of the plume with the cratonic lithosphere. In contrast, the Younger Extrusives as exemplified by the Oldoinyo Lengai nephelinite–carbonatite volcanism could be derived from this ancient metasomatized lithospheric mantle plus a recent plume-derived asthenospheric component and no contamination by crustal material. The genetically distinct Natron–Engaruka melilitites are considered to represent direct adiabatic melting of the Tanzanian plume without lithospheric contributions.

Further investigations at Mosonik should include a more extensive sampling of the eroded edifice; characterization of the large blocks of lava in the debris flows of the Leshuta River Gorge; and the petrology of the suite of ijolite series xenoliths. Clearly, given the paucity of geological, petrological and isotopic studies of all the volcanoes of the North Tanzanian Divergence, especially the basaltic basal sequences, coupled with the current ambiguity regarding their genesis, many further investigations are desirable before any comprehensive petrogenetic scheme for this province can be formulated.

https://doi.org/10.1017/S0016756822000619 Published online by Cambridge University Press

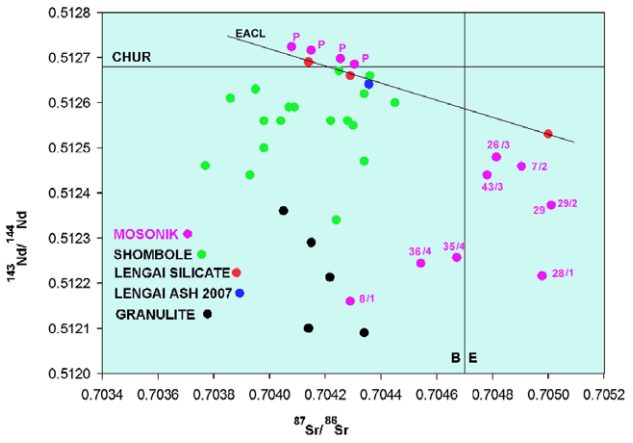

Fig. 15. (Colour online) ^{143}Nd/^{144}Nd versus ^{87}Sr/^{86}Sr correlation diagram for lavas from Mosonik (this work; Paslick *et al*. 1996), Shombole (Bell & Peterson, 1991) and Lengai silicate lavas (Bell & Dawson, 1995). Data for granulite xenoliths are from (Cohen *et al*. 1984), and the East African Carbonatite Line (EACL) from Bell & Blenkinsop (1987). Mosonik samples are labelled as 'sample number/lava type' i.e. 8/1, or P for data from Paslick *et al*. (1996).

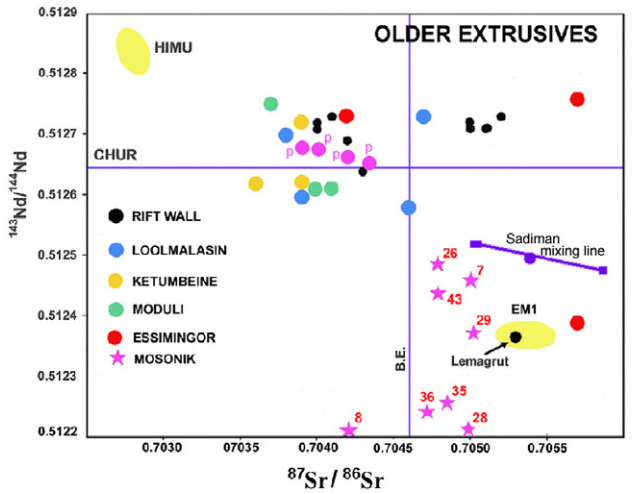

Fig. 16. (Colour online) ^{143}Nd/^{144}Nd versus ^{87}Sr/^{86}Sr correlation diagram for Old Extrusive Series lavas from Mosonik (this work; Paslick *et al*. 1995, 1996; Mana *et al*. 2012, 2015) and Sadiman (Zaitsev *et al*. 2019). Labels for Mosonik lavas as in Figure 15.

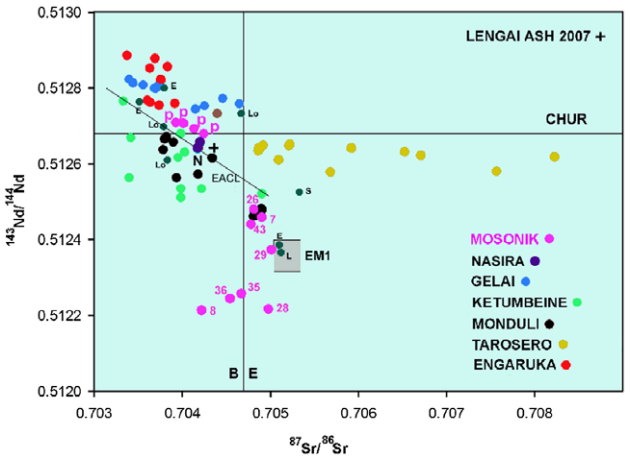

Fig. 17. (Colour online) ^{143}Nd/^{144}Nd versus ^{87}Sr/^{86}Sr correlation diagram for lavas from the Engaruka volcanic field and Mosonik (this work; Paslick *et al*. 1996) compared with other volcanic rocks of the Older and Newer Extrusive Series (Paslick *et al*. 1995, 1996; Mana *et al*. 2012, 2015). Labels for Mosonik lavas as in Figure 15; E – Essimingor; L – Lemagrut; Lo – Loolmalasin; N – Nasira; S – Sadiman. Data for Nasira and Lengai 2007 ash (this work). EACL – East African Carbonatite Line (Bell & Blenkinsop (1987); BE – bulk earth ^{87}Sr/^{86}Sr ratio (0.7047); CHUR = ^{143}Nd/^{144}Nd ratio of 0.512638.

Supplementary material. To view supplementary material for this article, please visit https://doi.org/10.1017/S0016756822000619

Acknowledgements. This work is presented as a memorial to the late John Barry Dawson (1932–2013), my companion on several expeditions to the volcanic rocks of the North Tanzanian Divergence. This investigation of Mosonik was initiated during 2006–2009 subsequent to our expedition to this volcano in 2005, but unfortunately the dissemination of our resulting mineralogical and geochemical investigations were interrupted by Barry's untimely passing. This work was supported financially by the Natural Sciences and Research Council of Canada, Lakehead University and Almaz Petrology. On several expeditions to the Engaruka region of Tanzania the logistics were expertly managed by Dorobo Safaris of Arusha and their field staff Alex, Peter and Lomnyak. Anatoly Zaitsev, Michael Marks and an anonymous reviewer are thanked for useful comments on, and reviews, of this work. Valerie Dennison is thanked for editorial assistance.

Conflict of interest. None.

References

Ablay GJ, Carroll MR, Palmer MR, Marti J and Sparks RSJ (1998) Basanite-phonolite lineages of the Teide-Pico Viejo volcanic complex, Tenerife, Canary Islands. *Journal of Petrology* **39**, 905–36

Baker BH, Mohr PA and Williams LAJ (1972) *Geology of the Eastern Rift System of Africa*. Geological Society of America, Special Papers vol. 136.

Baudouin C, Parat F, Denis CMM and Mangasini M (2016) Nephelinite lavas at early stage of rift initiation (Hanang volcano, North Tanzanian Divergence). *Contributions to Mineralogy and Petrology* **171**, 14. doi: 10.1007/s00410-016-1273-5.

Bell K and Blenkinsop J (1987) Nd and Sr isotopic composition of East African carbonatites: implications for mantle heterogeneity. *Geology* **15**, 99–102.

Bell K and Dawson JB (1995) Nd and Sr isotope systematics of the active volcano, Oldoinyo Lengai. In *Carbonatite Volcanism of Oldoinyo Lengai and Petrogenesis of Natrocarbonatite* (eds K Bell and J Keller), pp. 100–12. Berlin: Springer Verlag.

Bell K and Peterson TD (1991) Nd and Sr isotope systematics of Shombole volcano, East Africa, and the links between nephelinites, phonolites, and carbonatites. *Geology* **19**, 582–5.

Berger J, Ennih H, Mercier J-CC, Liégeois J-P and Demaiffe D (2009). The role of fractionation and late stage peralkaline melt segregation in the mineralogical evolution of Cenozoic nephelinites/phonolites from Saghro (SE Morocco). *Mineralogical Magazine* **73**, 59–82.

Boynton WV (1985) Geochemistry of the rare earth elements: meteorite studies. In *Rare Earth Element Geochemistry* (ed. P Henderson), pp. 115–52. Developments in Geochemistry 2. Amsterdam: Elsevier.

Braunger S, Marks MAW, Wenzel T, Zaitsev AN and Markl G (2021) The petrology of the Tarosero volcanic complex: constraints on the formation of extrusive agpaitic rocks. *Journal of Petrology* **62**, egab015. doi: 10.1093/petrology/egab015.

Brey G (1978) Origin of olivine melilitites – chemical and experimental constraints. *Journal of Volcanology and Geothermal Research* **3**, 61–88.

Brögger WC (1921) *Die Eruptivgesteine des Kristianagebietes. IV. Das Fengebeit in Telemark, Norwegen*. Oslo: Norsk Videnskaps Skrifter Matematisk–Nature Vitenskapelig Klasse No. 9.

Bryan SE, Marti J and Leossan M (2002) Petrology and geochemistry of the Bandas del Sur Formation, Las Cañadas, (Canary Islands). *Journal of Petrology* **43**, 1815–56.

Cohen RS, O'Nions RK, and Dawson JB (1984) Isotope geochemistry of xenoliths from East Africa: implications for the development of mantle reservoirs and their interaction. *Earth and Planetary Sciences* **68**, 209–20.

Dawson JB (2008) *The Gregory Rift Valley and Neogene–Recent Volcanoes of Northern Tanzania*. Geological Society of London, Memoir no. 33, 102 pp.

Dawson JB and Powell DG (1969) The Engaruka-Natron explosion crater area, northern Tanzania. *Bulletin Volcanologique* **33**, 791–817.

Droop GTR (1987) A general equation for estimating Fe^{3+} concentrations in ferromagnesian silicates and oxides from microprobe analyses using stoichiometric criteria. *Mineralogical Magazine* **51**, 431–5.

Emeleus CH and Troll VR (2014) The Rum Igneous Centre, Scotland. *Mineralogical Magazine* **78**, 805–39.

Fairhead JD, Mitchell JG and Williams LAJ (1972) New K/Ar determinations on rift volcanics of S. Kenya and their bearing on the age of rift faulting. *Nature* **238**, 66–9.

Floess D, Caricchi L, Simpson G and Wallis SR (2019) Melt segregation and the architecture of magmatic reservoirs: insights from the Muroto sill (Japan). *Contributions to Mineralogy and Petrology* **174**, 27–42.

Guest NJ, James TC, Pickering R and Dawson JB (1961) Angata Salei. Tanzania Geological Survey Quarter Degree Sheet 40.

Hepworth LN, Kaufmann FED, Hecht L, Gertisser R and O'Driscoll B (2020) Braided peridotite sills and metasomatism in the Rum Layered Suite, Scotland. *Contributions to Mineralogy and Petrology* **175**, 1–25.

Isaac GL and Curtis GH (1974) Age of the Acheulian industries from the Peninj Group, Tanzania. *Nature* **249**, 624–7.

Keller J, Zaitsev AN and Wiedenmann D (2006) Primary magmas at Oldoinyo Lengai: the role of olivine melilitites. *Lithos* **91**, 150–72.

Le Maitre RW, Streckeisen A, Zanettin B, Le Bas MJ, Bonin B, Bateman P, Bellieini G, Dudek A, Efremova S, Keler J, Lameyre J, Sabine PA, Schmid R, Sørensen H and Woolley AR (2002) *Igneous Rocks: A Classification and Glossary of Terms: Recommendations of the IUGS Subcommission on the Systematics of Igneous Rocks*. New York: Cambridge University Press.

Locock AJ (2008) An Excel spreadsheet to recast analyses of garnet into end-member components, and a synopsis of the crystal chemistry of natural silicate garnets. *Computers and Geoscience* **34**, 1769–80.

Mana S, Furman T, Carr MJ, Mollel GF, Mortlock RA, Feigensen MD, Turrin BD and Swisher CC (2012) Geochronology and geochemistry of the Essimingor volcano: melting of metasomatized lithospheric mantle beneath the North Tanzanian Divergence zone (East African Rift). *Lithos* **155**, 310–25.

Mana S, Furman T, Turrin BD, Feigenson MD and Swisher CC (2015) Magmatic activity across the East African North Tanzanian Divergence Zone. *Journal of the Geological Society, London* **172**, 368–9.

Mattsson HB, Nandedkar RH and Ulmer P (2013) Petrogenesis of the melilititic and nephelinitic rock suites in the Natron-Engaruka monogenetic volcanic field, northern Tanzania. *Lithos* **179**, 175–92.

Mitchell RH (1972) Composition of nepheline, pyroxene and biotite in ijolite from the Seabrook Lake complex, Ontario. *Neues Jahrbuch für Mineralogie Monatshefte* **9**, 415–22.

Mitchell RH (2009) Peralkaline nephelinite-natrocarbonatite immiscibility and carbonatite assimilation at Oldoinyo Lengai, Tanzania. *Contributions to Mineralogy and Petrology* **158**, 589–98.

Mitchell RH and Dawson JB (2007) The September 24th, 2007, ash eruption of the carbonatite volcano, Oldoinyo Lengai, Tanzania: mineralogy of the ash and implications for the formation of a new hybrid magma type. *Mineralogical Magazine* **71**, 483–92.

Mitchell RH and Platt RG (1982) Mineralogy and petrology of nepheline syenites from the Coldwell alkaline complex, Ontario, Canada. *Journal of Petrology* **23**, 186–214.

Mitchell RH and Platt RG (1984) The Freemans Cove volcanic suite; field relations, petrochemistry and tectonic setting of nephelinite-basanite volcanism associated with rifting in the Canadian Arctic Archipelago. *Canadian Journal of Earth Sciences* **21**, 428–36.

Mitchell RH and Vladykin NV (1996) Compositional variation of pyroxene and mica from the Little Murun ultrapotassic complex, Aldan Shield, Russia. *Mineralogical Magazine* **69**, 907–25.

Muirhead JD, Kattenhorn SA, Lee H, Mana S, Turrin BD, Fischer TP, Kianji G, Dindi E and Stamps DS (2016) Evolution of upper crustal faulting assisted by magmatic volatile releases during early-stage continental rift development in the East African Rift. *Geosphere* **12**, 1670–700.

Paslick CR, Halliday AN, James D and Dawson JB (1995) Enrichment of the continental lithosphere by OIB melts: isotopic evidence from the volcanic province of northern Tanzania. *Earth and Planetary Science Letters* **130**, 109–26.

Paslick CR, Halliday AN, Langem RA, James D and Dawson JB (1996) Indirect crustal contamination: evidence from alkali basalts and nephelinites from Northern Tanzania. *Contributions to Mineralogy and Petrology* **125**, 277–92.

Peterson TD (1989a) Peralkaline nephelinites I. Comparative petrology of Shombole and Oldoinyo Lengai, East Africa. *Contributions to Mineralogy and Petrology* **101**, 458–78.

Peterson TD (1989b) Peralkaline nephelinites. II. Low pressure fractionation and the hypersodic lavas of Oldoinyo Lengai. *Contributions to Mineralogy and Petrology* **102**, 336–46.

Reiss MC, Muirhead JD, Laizer AS, Link E, Kazimoto EO, Ebinger CJ and Rümpker C (2021) The impact of complex volcanic plumbing on the nature of seismicity in the developing magmatic Natron Rifting, Tanzania. *Frontiers in Earth Science* **8**, 609805. doi: 10.3389/feart.2020.609805.

Rogers NW, Hawkesworth CT and Palacz ZA (1992) Phlogopite in the generation of olivine melilitites from Namaqualand, South Africa and implications for element processes in the mantle. *Lithos* **28**, 347–65.

Rosenbusch H (1907) *Mikroskopische Physiographie der Mineralien und Gesteine*, 4th Edition. Stuttgart: E. Schweizerbart'sche.

Savard JJ and Mitchell RH (2021) Petrology of ijolite series rocks from the Prairie Lake (Canada) and Fen (Norway) alkaline rock-carbonatite complexes. *Lithos* **396–397**, 106188. doi: 10.1016/j.lithos.2021.106188.

Sedova AM, Zaitsev AN and Spratt J (2018) The mineralogy of the effusive silicate rocks from the Mosonik volcano, Northern Tanzania. In *Proceedings of the International Conference on Magmatism of the Earth and Related Strategic Metal Deposits, 3–7 September 2018*, pp. 268–9. Moscow: Vernadsky Institute of Geochemistry and Analytical Chemistry of Russian Academy of Sciences.

Uhlig C (1907) Der sogennante grosse Ostafrikanische Graben zwischen Magad (Natron See) und Lawa ya Mweri (Manyara See). *Geographisches Zeitung* **15**, 478–505.

Uhlig C and Jaeger F (1942) Die Ostafrikannische Bruchstufe and die angrgenzenden Gebiete zwischen die Seen Magad und Lawa ja Meri sowie den Westfuss des Meru. Deutschen Instituts für Länderkunde, Wissenschaften Veröffentlichungen, Neue Folge 10, 284 pp.

Weeraratne DS, Forsyth DW, Fischer M and Nyblade A (2003) Evidence for an upper mantle plume beneath the Tanzanian craton from Rayleigh wave tomography. *Journal of Geophysical Research: Solid Earth* **108**, B9. doi: 10.1029/2002JB002273.

Zaitsev AN, Marks MAW, Wenzel T, Spratt J, Sharygin VV, Strekopytov S and Markl G (2012) Mineralogy, geochemistry and petrology of the phonolitic to nephelinitic Sadiman volcano, Crater Highlands, Tanzania. *Lithos* **152**, 66–83.

Zaitsev AN, McHenry L, Savchenok AI, Strekopytov S, Sprat J, Humphreys-Williams E, Sharygin VV, Bogomolov ES, Chakhmouradian AR, Zaitseva OA, Arzamastsev AA, Reguire EP, Leach L, Leach M and Mwankunda J (2019) Stratigraphy, mineralogy and geochemistry of the Upper Laetolil tuffs including a new tuff 7 site with footprints of *Australopithecus afarensis*, Laetolil, Tanzania. *Journal of African Earth Sciences* **158**, 103561. doi: 10.1016/j.jafrearsci.2019.103561.

Zaitsev AN, Spratt J, Shaygin VV, Wenzel T, Zaitseva OA and Markl G (2015) A comparison with possible volcanic sources from the Crater Highlands and Gregory Rift. *Journal of African Earth Sciences* **111**, 214–21.